

IMAGING INFRARED SEEKER DESIGN

A THESIS SUBMITTED TO  
THE GRADUATE SCHOOL OF NATURAL AND APPLIED SCIENCES  
OF  
MIDDLE EAST TECHNICAL UNIVERSITY

BY

AHMET ÜNAL

IN PARTIAL FULFILLMENT OF THE REQUIREMENT  
FOR  
THE DEGREE OF MASTER OF SCIENCE  
IN  
PHYSICS

JUNE, 2014



Approval of the thesis:

**IMAGING INFRARED SEEKER DESIGN**

submitted by **AHMET ÜNAL** in partial fulfillment of the requirements for the degree of **Master of Science in Physics Department, Middle East Technical University** by,

Prof. Dr. Canan Özgen

Dean, Graduate School of **Natural and Applied Sciences** \_\_\_\_\_

Prof. Dr. Mehmet T. Zeyrek

Head of Department, **Department of Physics** \_\_\_\_\_

Assoc. Dr. Serhat Çakır

Supervisor, **Department of Physics, METU** \_\_\_\_\_

**Examining Committee Members**

Assoc. Prof. Dr. İsmail Rafatov

Department of Physics, METU \_\_\_\_\_

Assoc. Prof. Dr. Serhat Çakır

Department of Physics, METU \_\_\_\_\_

Assist. Prof. Dr. Kemal Efe Eseller

Department of Electrical & Electronic Engineering, \_\_\_\_\_

Atılım University

Assoc. Prof. Dr. Burak Yedierler

Department of Physics, METU \_\_\_\_\_

Assist. Prof. Dr. Alpan Bek

Department of Physics, METU \_\_\_\_\_

**Date :** 30.06.2014

**I hereby declare that all information in this document has been obtained and presented in accordance with academic rules and ethical conduct. I also declare that, as required by these rules and conduct, I have fully cited and referenced all material and results that are not original to this work.**

Name, Last Name: Ahmet ÜNAL

Signature :

## **ABSTRACT**

### **IMAGING INFRARED SEEKER DESIGN**

Ünal, Ahmet

M. Sc., Department of Physics

Supervisor: Assoc. Prof. Dr. Serhat Çakır

June 2014, 78 pages

The subject of this study is the design of an imaging infrared seeker for aerial targets. Firstly the radiant power of the target was discussed and optical design of seeker lenses were done with ZEMAX Optical Design Software considering the MTF (Modulation Transfer Function) values, optical path differences, distortions and detection range calculations. After that, detection range calculations and simulation results of the optical system were presented.

Before lock on range calculations, spectral band of the system was analyzed and chosen for aerial targets. After that, lock on range was calculated considering detector noise, background noise and target radiation. Afterward the optical parameters of the seeker were determined. Focal length and  $F_{\#}$  (F-number) of the seeker was calculated as it was receiving the aerial target and background radiation at 5 km distance. Design was done using ZEMAX optical design program. Moreover, the lens materials were Silicon, Germanium and Cadmium Selenide and Sapphire were dome material. Finally, optical performance parameters have been analyzed.

Finally, test plate fitting is applied to the optical system. Manufacturing parameters were presented and discussed.

**Keywords:** Infrared Imaging, IIR, Optical Design, ZEMAX, MWIR, Infrared Seeker.

## ÖZ

### KIZILÖTESİ ARAYICI BAŞLIK TASARIMI

Ünal, Ahmet

Yüksek Lisans, Fizik Bölümü

Tez Yöneticisi : Doç. Dr. Serhat Çakır

Haziran 2014, 78 sayfa

Bu çalışmada hava hedefleri için kızılötesi arayıcı başlık tasarımı amaçlanmıştır. İlk olarak hedefin kızılötesi ışınım gücü tartışılmıştır ve daha sonra MTF değerleri, optik yol farkları, distorsiyon ve hedefi algılama mesafesi dikkate alınarak ZEMAX programı ile optik sistem tasarımı yapılmıştır. Daha sonra, hedefi algılama hesapları ve optik tasarımın sonuçları sunulmuştur.

Hedefe kilitlenme mesafesi hesaplamalarından önce hedefin spektral bant aralığı analiz edilmiş ve hedef seçilmiştir. Daha sonra, detektör gürültüsü, arka plan gürültüsü ve hedef ışınması dikkate alınarak hedefe kilitlenme mesafesi hesaplanmış, arayıcı başlığın optik parametreleri belirlenmiştir. Arayıcı başlığın odak uzunluğu ve  $F_{\#}$  (F numarası), hedef ve arka plan ışınmasını 5 km mesafen alıyormuş gibi hesaplanmıştır. Lens malzemeleri silikon, germanyum ve kadmiyum selenit, dom malzemesi olarak da safir seçilmiştir. Son olarak, optik performans parametreleri analiz edilmiştir.

Sonuç olarak test plakaları analizi optik sisteme uygulanmıştır. Üretim parametreleri sunulmuş ve tartışılmıştır.

**Anahtar Kelimeler:** Kızılötesi Görüntüleyici, IIR, Optik Tasarım, ZEMAX, MWIR, Kızılötesi Arayıcı Başlık.

*To My Parents*

## ACKNOWLEDGEMENTS

First of all, I would like to thank my supervisor Assoc. Prof. Dr. Serhat AKIR for his kind guidance, cooperation, encouragement and advice throughout the study.

I would like to thank to Prof. Dr. Mehmet T. ZEYREK and Assoc. Prof. Dr. Hakan ALTAN for their support for admission to Department of Physics.

I sincerely thank to RST Uzaktan Algılama ve Gv. Tekn. Bil. Elk. Dan. Mh. Mim. Tic. A.Ş. and the managers for giving me the chance to complete my Master of Science degree.

Finally, I would like to thank my family for their continuous support and encouragement through all my life.

## TABLE OF CONTENTS

ABSTRACT.....	v
ÖZ .....	vii
ACKNOWLEDGEMENTS .....	x
TABLE OF CONTENTS .....	xi
LIST OF TABLES .....	xiii
LIST OF FIGURES .....	xiv
LIST OF ABBREVIATIONS .....	xvii
CHAPTERS	
1. INTRODUCTION.....	1
2. BACKGROUND INFORMATION.....	3
2.1 The Electromagnetic Spectrum .....	3
2.2 The Atmospheric Transmittance .....	4
2.3 Radiometry & Thermal Radiation .....	5
2.4 Signature Estimation of an Aircraft.....	11
2.5 Optical Design Parameters .....	12
2.5.3 Diffraction, Aberrations and Image Quality .....	14
2.6 Detector Parameters.....	26
3. DEVELOPMENT OF HEAT SEEKERS .....	29
3.1 Infrared Seekers.....	31
3.1.1 First Generation Infrared Seekers .....	31
3.1.2 Second Generation Infrared Seekers .....	33
3.1.3 Third Generation Infrared Seekers .....	34
3.2 Imaging Infrared Seekers .....	35
3.2.1 Scanning Infrared Seekers .....	36

3.2.2 Staring Infrared Seekers.....	37
3.2.3 Dual Band Staring Infrared Seekers .....	38
4. SYSTEM DESIGN.....	39
4.1 Detection Range Calculations.....	39
4.2 Optical Design of Seeker Objective .....	45
4.3 Optical System Performance Parameters.....	60
5. DISCUSSION AND CONCLUSION .....	67
REFERENCES.....	71
APPENDICES	
A. SOFTWARE CODES OF “INFRARED RANGE AND NETD CALCULATOR” .....	75

## LIST OF TABLES

### TABLES

Table 1.1 Emissivity values at 300 K [3].....	9
Table 4.1 Detector parameters [17].....	41
Table 4.2 Optical parameters .....	46
Table 4.3 Lens parameters for case 1 .....	47
Table 4.4 Lens parameters for case 2.....	49
Table 4.5 Lens parameters for case 3.....	51
Table 4.6 Lens parameters for case 4.....	53
Table 4.7 Lens parameters for case 5.....	55
Table 4.8 Lens parameters for case 6.....	57
Table 4.9 Lens parameters for case 7.....	59
Table 5.1 Lens parameters after test plate fitting.....	68

## LIST OF FIGURES

### FIGURES

Figure 2.1 Electromagnetic spectrum and infrared sub regions [2] .....	4
Figure 2.2 Atmospheric transmittance in infrared region [6].....	5
Figure 2.3 Schematic representation of Kirchhoff's law .....	6
Figure 2.4 Spectral radiance exitance versus wavelength graph.....	8
Figure 2.5 Different types of emissivity.....	8
Figure 2.6 Solid angle model .....	10
Figure 2.7 An aircraft model [4] .....	11
Figure 2.8 Lens parameters .....	12
Figure 2.9 Optical system specifications.....	14
Figure 2.10 Focus points of a) theoretical and b) real lenses.....	15
Figure 2.11 Spherical aberration .....	16
Figure 2.12 Reducing spherical aberration .....	16
Figure 2.13 Optical aberration of a) coma, b) spot size of different fields. ....	17
Figure 2.14 Different aperture stop positions are shown in a) coma with stop in front of lens, b) reduced coma with stop after lens .....	18
Figure 2.15 Astigmatism [15] .....	20
Figure 2.16 Field curvature .....	20
Figure 2.17 Distortion .....	21
Figure 2.18 Chromatic aberrations a) Longitudinal chromatic aberration b) Lateral chromatic aberration.....	22
Figure 2.19 Optical path difference (OPD).....	23
Figure 2.20 Image of a point source with different optical path difference due to coma .....	24
Figure 2.21 Meaning of the modulation transfer function .....	25
Figure 2.22 Typical MTF curves.....	26
Figure 3.1 Schematic representation of a heat seeker and target (FOV; Field of view) .....	30

Figure 3.2 Heat seekers block diagram .....	30
Figure 3.3 Reticle structure and the detector output pulse [11] .....	32
Figure 3.4 Optical structure of the 1. generation infrared seekers [12] .....	33
Figure 3.5 Time domain analysis a) no target, b) target, c) target in different angular position than case b).....	33
Figure 3.6 Structure and Its output of the con-scan reticle seeker [12] .....	34
Figure 3.7 Optical structure of the rosette scanning infrared seeker ( $f_1$ and $f_2$ rotating frequencies of prisms) .....	35
Figure 3.8 Working geometry of the rosette-scan seekers [14] .....	35
Figure 3.9 Schematic representation of scanning infrared seeker optic.....	36
Figure 3.10 Optical representation of refractive imaging infrared seeker .....	37
Figure 3.11 Optical representation of reflective imaging infrared seeker .....	38
Figure 4.1 Spectral radiant exitance graph for a) 750 K,600 K and 500 K objects, b) background 300 K object .....	40
Figure 4.2 Cold shield and F/# .....	42
Figure 4.3 Infrared range and NETD calculator software interface.....	43
Figure 4.4 Background dimension calculation.....	44
Figure 4.5 Solid angle calculations. ....	45
Figure 4.6 FOV calculation for optical system .....	46
Figure 4.7 Zemax simulations for case 1; a) optical system, b) spot sizes for different fields.....	48
Figure 4.8 Zemax simulations for case 2; a) optical system, b) spot sizes for different fields.....	50
Figure 4.9 Zemax simulations for case 3; a) optical system, b) spot sizes for different fields.....	52
Figure 4.10 Zemax simulations for case 4; a) optical system, b) spot sizes for different fields. ....	54
Figure 4.11 Zemax simulations for case 5; a) optical system, b) spot sizes for different fields. ....	56
Figure 4.12 Zemax simulations for case 6 ; a) optical system, b) spot sizes for different fields. ....	58

Figure 4.13 Zemax simulations for case 7; a) optical system, b) spot sizes for different fields. ....	60
Figure 4.14 OPD of the optical system a) 0° field, b) 3° field and c) 3.7° field .....	62
Figure 4.15 Distortion of the optical system .....	64
Figure 4.16 MTF of the optical system .....	66

## LIST OF ABBREVIATIONS

AM	: Amplitude Modulation
AP	: Amplitude Phase Modulation
ATA	: Automatic Target Acquisition
ATR	: Automatic Target Recognition
CA	: Clear Aperture
CT	: Center Thickness
EFL	: Effective Focal Length
ET	: Edge Thickness
FOR	: Fields of Regard
FOV	: Field of View
FP	: Frequency Phase Modulation
IFOV	: Instantaneous Field of View
IIR	: Imaging Infrared
InSb	: Indium Antimonite
IR	: Infrared
LWIR	: Long Wave Infrared
MTF	: Modular Transfer Function
MWIR	: Mid Wave Infrared
NIR	: Near Infrared
OPD	: Optical Path Difference
SNR	: Signal to Noise Ratio
SWIR	: Short Wave Infrared



## CHAPTER 1

### INTRODUCTION

For surface to air missiles and air to air missiles, one of the examples of homing guidance is imaging infrared homing and it is used to detect the angular position of the target with respect to missile axis.

The objective of this study is to design an imaging infrared seeker. Seeker's spectral region is usually determined by the target radiation spectrum. In our case the target is an aircraft and it radiates in MWIR and LWIR regions of the electromagnetic spectrum due to the temperature of the object.

Detection range of a seeker is related with atmospheric transmission, background radiation, optical transmission of the optical components, F# (F-number) of the optical system and the noise of the detector [3]. Most popular imaging sensor materials in the MWIR range are HgCdTe (Mercury Cadmium Telluride), PbS (Lead Sulfide) and InSb (Indium Antimonide). An InSb detector array was used in this work. Other sensors may also be used instead of InSb detector.

Atmospheric transmission in infrared band is sensitive to the atmospheric conditions such as snow, rain, haze, smoke, dust and it depends on wavelength [3]. So the performance of the optical system or seeker depends on the atmospheric transmission conditions. In the world, many companies or scientific research labs use MODTRAN Software (Moderate Resolution Transmittance Code) to calculate the atmospheric transmission in related wavelength region. In this thesis, the atmospheric transmission will be taken from the literature.

The seeker was designed to detect a target at 5 km distance. Missile's diameter was assumed to be 140 mm and seeker's optics was assumed to be rotated as  $\pm 90^\circ$ . So the space requirement for the seeker optics was determined as 70 mm. Refractive optical components were used in the optical system. Rayleigh criteria and pixel pitch of the detector were taken into account for optical performance.

ZEMAX optical design program was used to reach the best performance. Lens parameters such as lens material, radius, thickness and distance between lenses were optimized for different cases. Generally, Hammer optimization was used in this work. Hammer optimization provides glass substitution. So that, lens conjugates that must be used in an optical design was determined by this method. Also the performance criterions like spot diagrams, MTF, distortion were discussed.

In the following chapters, the details of the study are presented.

In Chapter 2 basic definitions of infrared bands are given. The radiometric quantities are discussed for a typical aircraft. Basic definitions and brief information about optical system design are also given and system parameters are defined.

In Chapter 3 the heat seekers and heat seeker types are explained in working mechanisms. Future of heat seekers is also discussed.

In Chapter 4 the target radiation spectral band is determined by its temperature. After that lock on range calculation equations are carried out to find the detection range of a seeker at 5 km. The optical system requirements are determined. Finally optical system design was done using ZEMAX optical design software. Results were plotted and discussed.

In Chapter 5 the study is completed with discussion of the seeker and manufacturability of the system.

## CHAPTER 2

### BACKGROUND INFORMATION

#### 2.1 The Electromagnetic Spectrum

The electromagnetic spectrum is distribution of all possible electromagnetic radiation according to energy, frequency or it is the characteristic distribution of electromagnetic radiation emitted or absorbed by a particular object [3].

The electromagnetic spectrum is the electromagnetic waves from low frequencies (radio communication) to high frequencies (gamma radiation). Upper limit of electromagnetic spectrum for long wavelength is the universe and lower limit for short wavelength is in the vicinity of the Planck length [3, 7].

The electromagnetic spectrum is shown in Fig. 2.1 with infrared part between radio and visible waves. The infrared spectrum is divided into 5 sub regions, although this definition is arbitrary and it can change from one author to another [2].

The infrared region shown in Fig. 2.1 is based on a combination of the atmospheric transmittance and wavelength. In infrared region some subregions have better transmittance while other regions have no transmittance. The subregions or wavelength intervals that have better transmittance are called “*atmospheric windows*”. Infrared sensors or detectors are especially designed for these wavelength intervals. In this way, the near infrared (NIR) band is mostly used in fiber optic telecommunication systems, whilst the short wave infrared (SWIR) band allows to

work on long-distance telecommunications (remote sensing) using a combination of detector materials. The medium wavelength infrared (MWIR) and the long wavelength infrared (LWIR) bands find applications in infrared thermography for military or civil applications, *e.g.* target signature identification, surveillance, etc. The very long wavelength Infrared (VLWIR) band is used in spectroscopy and astronomy [2].

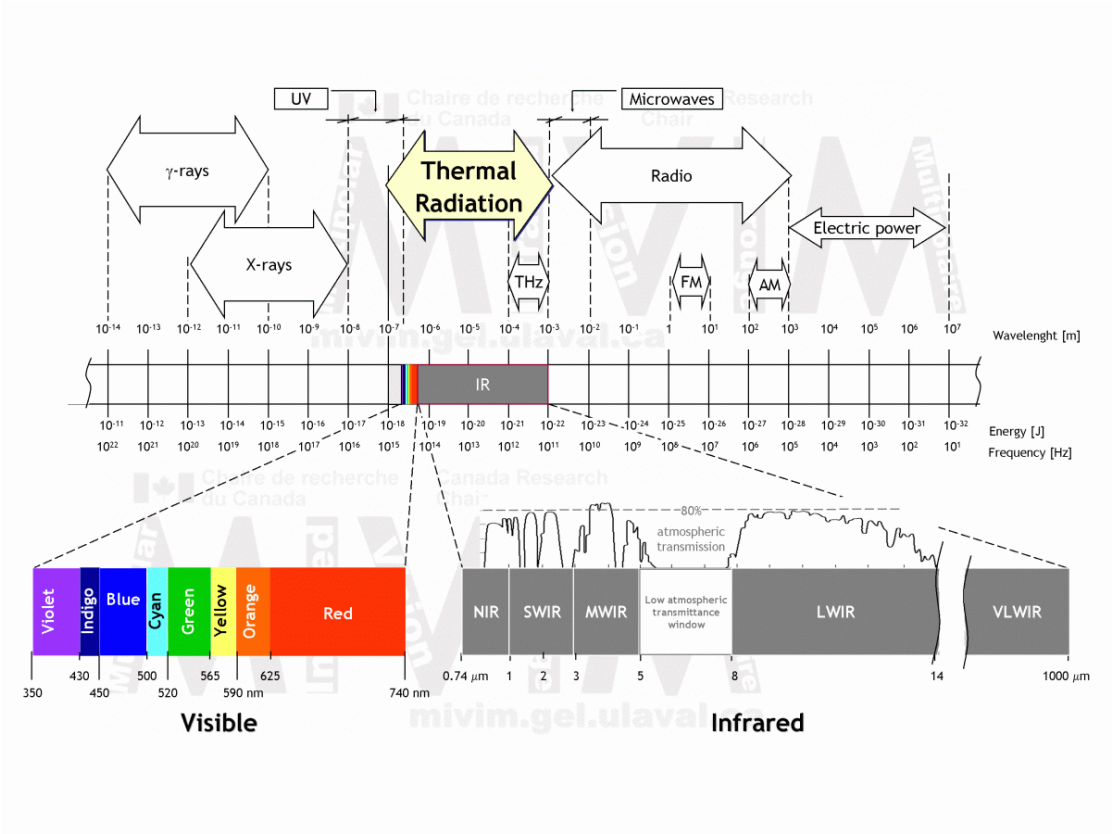


Figure 2.1 Electromagnetic spectrum and infrared sub regions [2]

### 2.2 The Atmospheric Transmittance

In Fig. 2.2, four of five main atmospheric windows of infrared: NIR, 0.74 to 1  $\mu\text{m}$ , SWIR, 1 to 3  $\mu\text{m}$ , MWIR, 3 to 5  $\mu\text{m}$  and LWIR, 8 to 14  $\mu\text{m}$  are shown. Most of the infrared systems use this band to develop infrared systems [2,3].

The atmosphere is a gaseous combination of CO<sub>2</sub>, H<sub>2</sub>O, N<sub>2</sub>, O<sub>2</sub> and O<sub>3</sub> molecules. Because of the molecular vibration of these, absorption attenuates the transmission of the infrared radiation. Attenuation also comes from the scattering by particles in the atmosphere. Fig. 2.2 shows the infrared bands and molecules that causes absorption. NIR and LWIR bands are affected by water vapor and MWIR band is affected by CO<sub>2</sub> and O<sub>3</sub> [2].

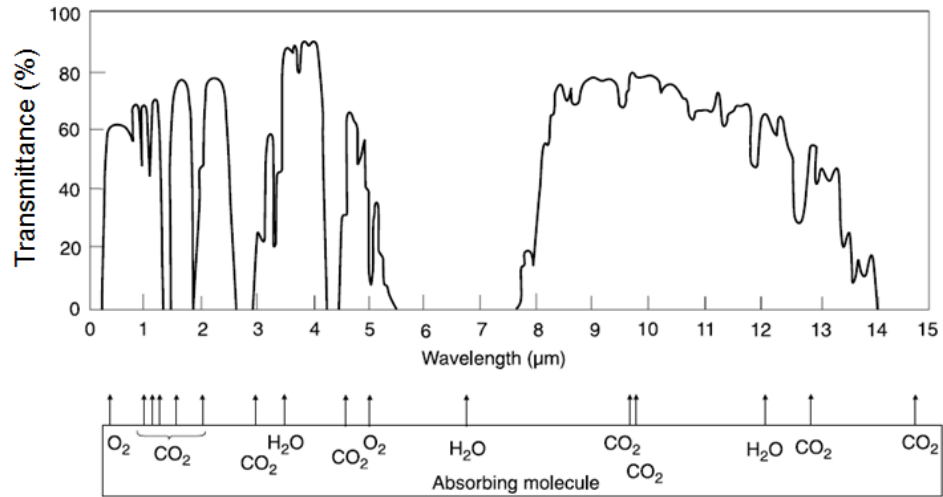


Figure 2.2 Atmospheric transmittance in infrared region [6]

Atmospheric transmittance is given by [9];

$$T(\lambda) = e^{-\sigma(\lambda)R} \quad (2.1)$$

where  $\sigma$  is called extinction coefficient determined by absorption and scattering and it is a function of wavelength. R is the distance (or range) to be calculated [20]. The equation shows the atmospheric transmittance of the weather and it is function of wavelength and range.

### 2.3 Radiometry & Thermal Radiation

Thermal radiation of very hot objects can be seen by human eye because the thermal emission of the object is in the visible region of the electromagnetic spectrum. As an

example, the Sun's temperature is approximately 6000 K and it can be seen by human eye. For objects at room temperature, the thermal radiation is in the infrared region. So, it can be seen by special detectors [7].

Radiometry is a quantitative analysis of flux from thermal radiation transfer between optical system and an emitter object. The radiated emission from an object transmits through the atmosphere and it is collected by optics. Radiometry is used to calculate the optical power that is needed to generate electrical signal on detector [3].

Total incident radiation that interacts with an object is equal to sum of absorbed, reflected and transmitted part of incident radiation or sum of Transmittance (T; transmitted energy over incident energy), Absorbance ( $\rho$ ; absorbed energy per incident energy) and Reflectance ( $\alpha$ ; reflected energy per incident energy) [3]. This is called Kirchhoff's Law. It can be formulized as

$$\alpha + \rho + T = 1 \tag{2.2}$$

It is also called thermal equilibrium and Kirchhoff's law is wavelength dependent absorption, emission at thermal equilibrium.

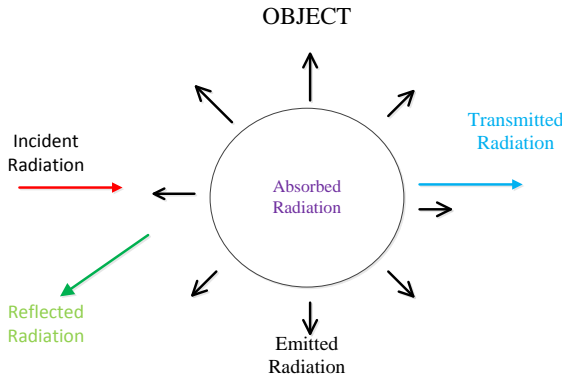


Figure 2.3 Schematic representation of Kirchhoff's law

Emissivity is a dimensionless quantity and it shows how much of the radiation is emitted from the object. It is equal to absorbed radiation of the object. If an object is good absorber, it is already a good emitter ( $\alpha = \varepsilon$  (emissivity), blackbody) [3].

When an object absorbs all incoming radiation strikes on it in all wavelengths, it is called “blackbody”. It does not transmit or reflect any part of the incident radiation. For blackbody  $\varepsilon = \alpha = 1$ ,  $\rho = 0$  and  $T = 0$ . Blackbody objects emit maximum radiation of the objects at any temperature [3].

“*Radiant Exitance*” is the radiant power from a surface per area and it is a function of temperature and wavelength. “*Spectral Radiant Exitance*” is the radiant power from a surface per area, per wavelength. The relation between spectral radiant exitance and radiant exitance is [3]

$$M = \int_{\lambda_1}^{\lambda_2} M_{\lambda} d\lambda \quad (2.3)$$

$M_{\lambda}$  is the symbol of the spectral radiant exitance and the unit is watt per area per wavelength and the  $M$  is the spectral radiant exitance and the unit is watt per unit area.  $\lambda_1$  and  $\lambda_2$  are the wavelength interval. Blackbody radiation can be specified by Planck’s equation is [3]

$$M_{\lambda, BB} = \frac{2\pi hc^2}{\lambda^5} \frac{1}{\exp\left(\frac{hc}{\lambda kT}\right) - 1} \quad (2.4)$$

where  $h$  is the Plank’s constant,  $k$  is the Boltzman’s constant,  $T$  is the temperature and  $c$  is the speed of light. Fig. 2.4 shows spectral radiance exitance versus wavelength corresponding to specific temperatures.

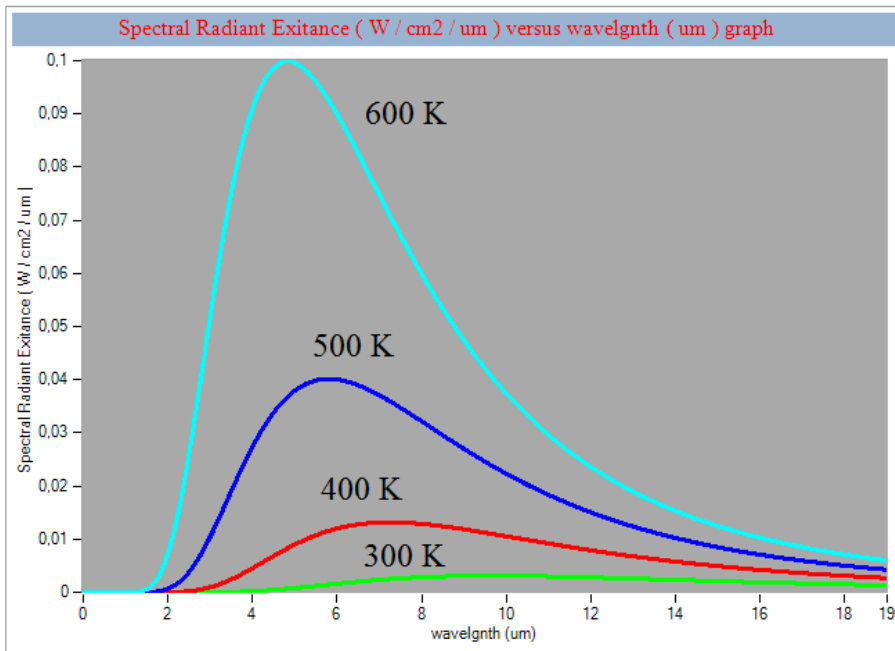


Figure 2.4 Spectral radiance exitance versus wavelength graph

When the emissivity  $\epsilon < 1$ , it is called grey body and some materials have emissivity that is a function of wavelength.

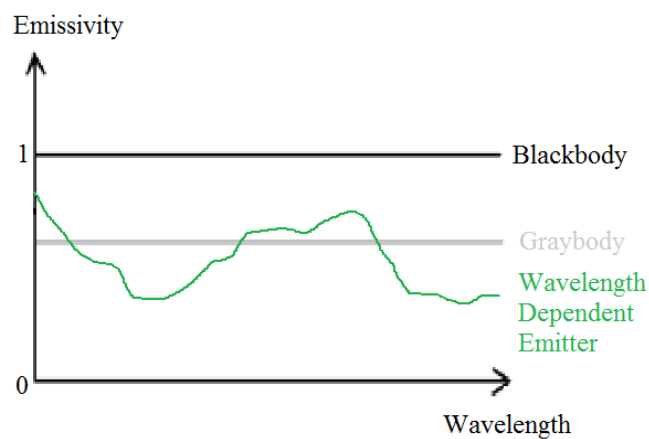


Figure 2.5 Different types of emissivity

Emissivity can be constant or a function of wavelength. Emissivity values of some materials are shown in the Table 1.

Table 1.1 Emissivity values at 300 K [3]

Material	Emissivity
Aluminum	0.05
Highly Polished Copper	0.02
Stainless Steel	0.16
Brick	0.93
Carbon	0.95
Glass	0.94
Sand	0.90
Human Skin	0.98
Distilled Water	0.96
Snow	0.90
Wood	0.9

By definition of blackbody, emissivity can be defined the ratio of spectral exitance of the object to the spectral exitance to the reference blackbody [3].

$$\varepsilon = \frac{M_{Object}}{M_{\lambda, BB}} = \frac{\int_0^{\infty} \varepsilon(\lambda) M_{\lambda}(\lambda, T) d\lambda}{\int_0^{\infty} M_{\lambda}(\lambda, T) d\lambda} \quad (2.5)$$

If the object is blackbody,  $\varepsilon$  is equal to 1. If not, then spectral radiance exitance is defined as

$$M_{Object} = \int_{\lambda_1}^{\lambda_2} \varepsilon(\lambda) M_{\lambda}(\lambda, T) d\lambda \quad (2.6)$$

Emissivity can be a constant or a function of wavelength for real objects.

“Solid angle” “ $\Omega$ ” is an angle in 3 dimensional space and it shows how large the object is seen from the observer position. It is dimensionless and measured in square

radians or steradians (sr) [3]. Fig. 2.6 shows the geometric representation of solid angle and it can be described as

$$\Omega = \frac{a}{r^2} \quad (2.7)$$

where  $a$  is the area of the surface on sphere and  $r$  is the distance from the source.

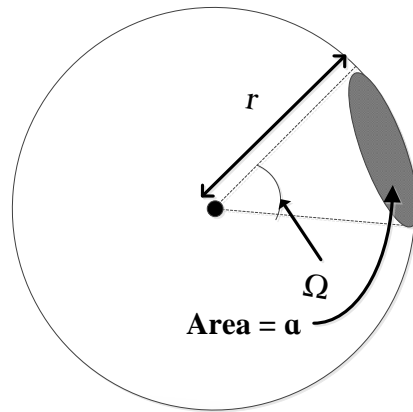


Figure 2.6 Solid angle model

Radiance exitance per unit solid angle is defined as “Radiance” and can be formulized as

$$M = \int L d\Omega = \int_0^{2\pi} d\phi \int_0^{\pi/2} L \sin \theta d\theta = \pi L$$

$$L = \frac{1}{\pi} \int_{\lambda_1}^{\lambda_2} M_{\lambda} d\lambda \quad (2.8)$$

where  $L$  is the radiance and unit is Watt per unit area per unit steradian and  $M_{\lambda}$  spectral radiance exitance for nonblackbody object but same equation can be written

for blackbody. In this situation  $M_\lambda$  will be  $M_{\lambda, BB}$  and radiance will be blackbody radiance [3].

## 2.4 Signature Estimation of an Aircraft

The signature of the target is variable from target to another target because every company's aerial vehicle has specific exitance from exhaust and remote sensing designers have to make an estimation to find the target signature model [9]. Fig. 2.7 shows an aircraft model for estimation of the target radiation. In Fig. 2.7 red parts shows hot parts of aircraft. Nose, engine inlets and leading edges cause from aerodynamic heats and exhaust plume comes from engine temperature.

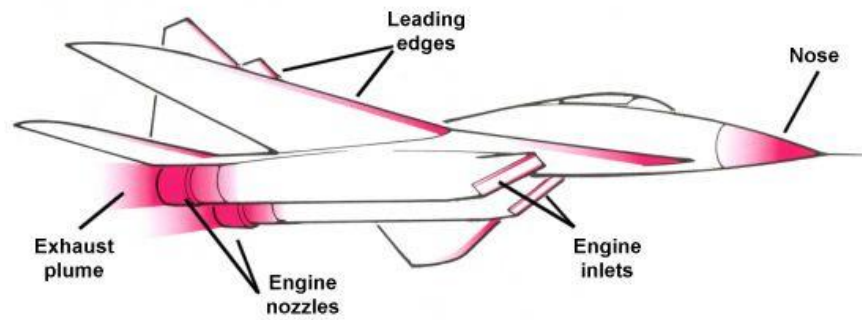


Figure 2.7 An aircraft model [4]

The target can be divided into  $n$  area elements where the radiance is uniform over each element. The total radiance that is emitted by the aircraft

$$L_{TOTAL} = \frac{1}{\pi} \sum_i^n \varepsilon_i \int_{\lambda_1}^{\lambda_2} M_{\lambda_i} d\lambda \quad (2.9)$$

where  $\varepsilon_i$  is emissivity of each element,  $M_{\lambda_i}$  is the spectral radiance exitance of each element and  $A_i$  is the area of the each element. Each element that shown in the Fig. 2.7 are in different temperatures and maximum radiation is emitted from engine

nozzles. There are many radiation sources such as plume, hot parts, skin, reflected sky shine, reflected earthshine, reflected clouds. These sources make an exact determination of the signature for an arbitrary aircraft virtually impossible. So, to make calculation simpler some assumptions has to done. The assumptions are

- The aerial platform is assumed to radiate as a gray body. In addition, the emissivity for all elements of the aircraft is assumed to be unity.
- The temperature is assumed to be uniform over sources.
- Aerodynamic heating effects are neglected.
- Maximum radiating element is considered as a main radiation source [9].

As a result the 2.9 can be simplified to

$$L_{TOTAL} = \frac{1}{\pi} \varepsilon \int_{\lambda_1}^{\lambda_2} M_{\lambda} d\lambda \quad (2.10)$$

where  $\lambda_1$  and  $\lambda_2$  are the wavelength limits of the infrared band.

## 2.5 Optical Design Parameters

Single lens and parameters are shown in Fig. 2.8.

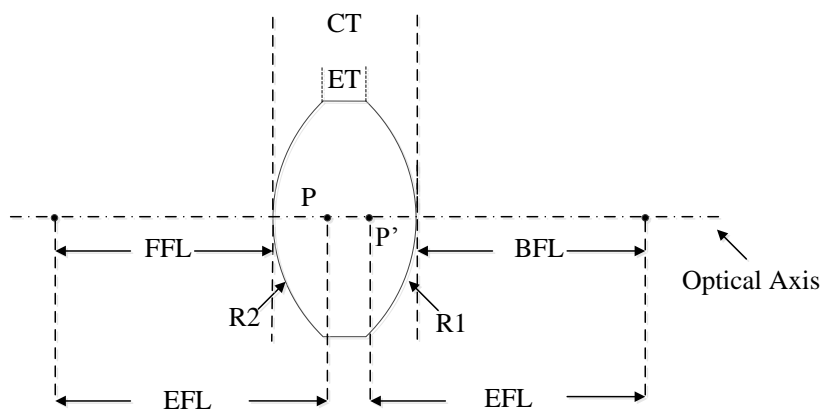


Figure 2.8 Lens parameters

$P$  is called front principle point of the lens and  $P'$  is called rear principle point. Plane that intersects principle point and optical axis is called principle plane of the lens. Plane that intersects  $P$  is called front principle plane and intersects  $P'$  is called rear principle plane.

$EFL$  is effective focal length of the lens and it is distance from rear principle plane to focal point of the lens.  $CT$  is center thickness and the  $ET$  is the edge thickness of the lens.  $BFL$  is back focal length and it is distance between rear surface of the lens on the optical axis and focal point.  $R_1$  is radius of the front surface and  $R_2$  is radius of the rear surface. Effective focal length of a thin lens is given as [22]

$$\frac{1}{EFL} = (n-1) \left( \frac{1}{R_1} - \frac{1}{R_2} \right) \quad (2.11)$$

where  $R_1$  and  $R_2$  are radius of first and second surface. For thick lens, effective focal length is [22]

$$\frac{1}{EFL} = (n-1) \left( \frac{1}{R_1} - \frac{1}{R_2} + \frac{(n-1)CT}{nR_1R_2} \right) \quad (2.12)$$

where  $n$  is the refractive index of lens material and  $CT$  is center thickness of the lens.

$F_{\#}$  or  $F$ -number is defined as focal length over clear aperture (it is called “entrance pupil diameter”).  $F_{\#}$  is given as

$$F_{\#} = \frac{EFL}{CA} \quad (2.13)$$

where  $EFL$  is the effective focal length and  $CA$  is the clear aperture. FOV (Field of view) is the angle with the optical system or lens accepts light [15].

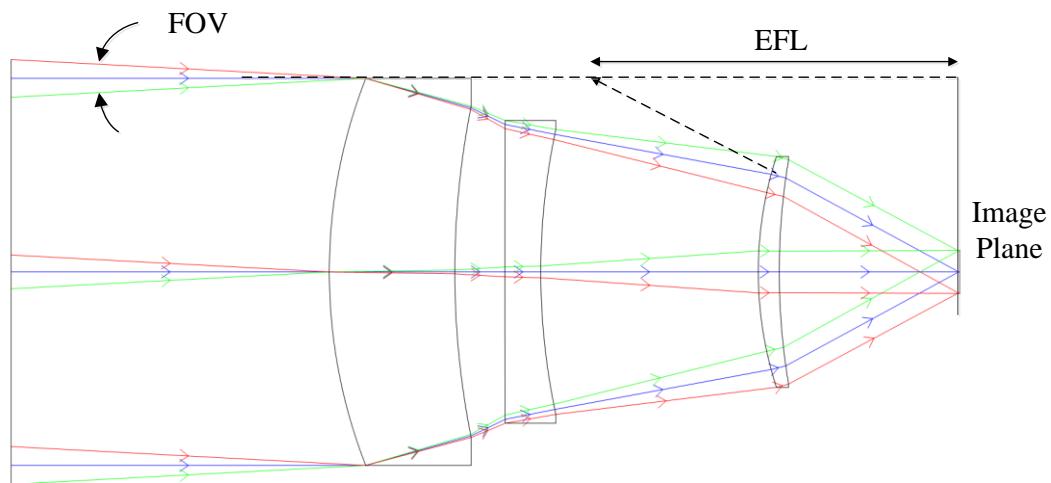


Figure 2.9 Optical system specifications

### 2.5.3 Diffraction, Aberrations and Image Quality

Aberrations are failure of the optical systems. For real lenses image quality is degraded by aberrations. Ideal and real focuses are shown in Fig. 2.10. “*Airy disc*” is called as an ideal spot size of an ideal lens and its diameter is given as  $2.44\lambda/CA$  where  $\lambda$  is wavelength.

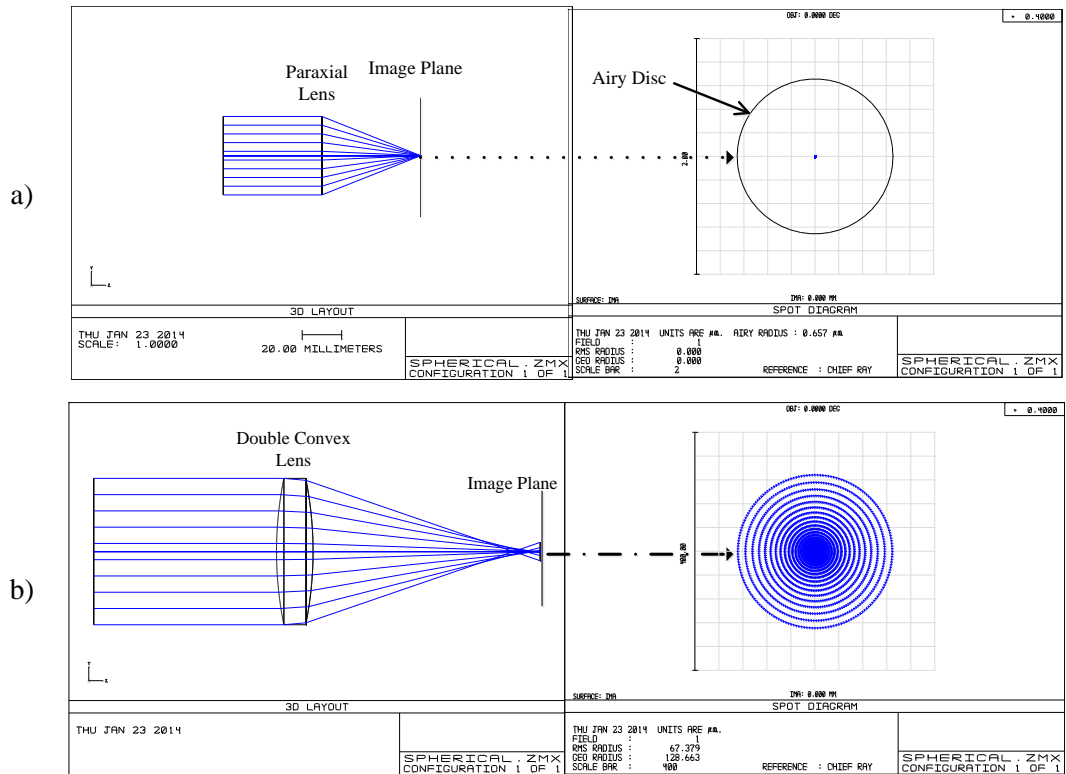


Figure 2.10 Focus points of a) theoretical and b) real lenses

For optical systems or single lenses, aberrations are failures of the optical system to produce an ideal focus in image plane. There are 6 known optical aberrations [15].

One of the aberrations is called “*spherical aberration*”. As shown in Fig. 2.11, when the ray height above the optical axis, the rays in image space cross the axis or focus closer and closer to the lens. This change of focus position in focal point is called spherical aberration.

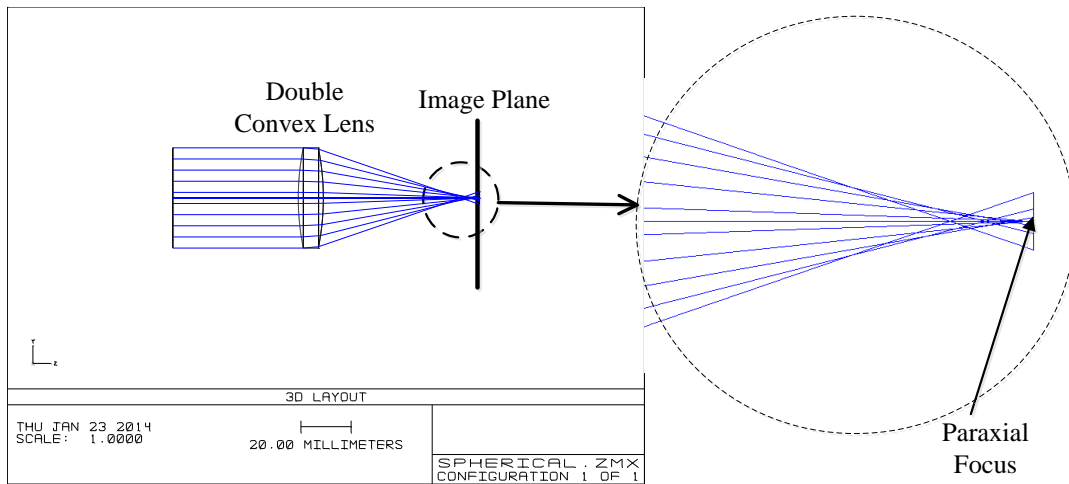


Figure 2.11 Spherical aberration

As shown in Fig. 2.12 spherical aberrations can be reduced by splitting the lens or lens bending [15].

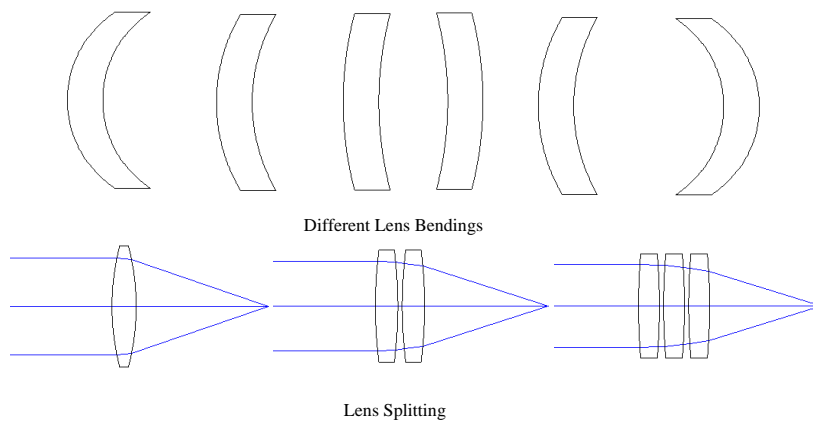


Figure 2.12 Reducing spherical aberration

For minimum spherical aberration for single lens  $R_1$  is given as [22]

$$R_1 = \frac{2(n+2)(n-1)}{n(2n+1)} EFL \quad (2.14)$$

for  $R_2$

$$R_2 = \frac{2(n+2)(n-1)}{n(2n-1)-4} EFL \quad (2.15)$$

Another optical aberration is called “coma”. If the rays enter to the lens with angle, this causes coma aberration. As shown in Fig. 2.13 every ray is focused by the lens to a certain height from the optical axis [15].

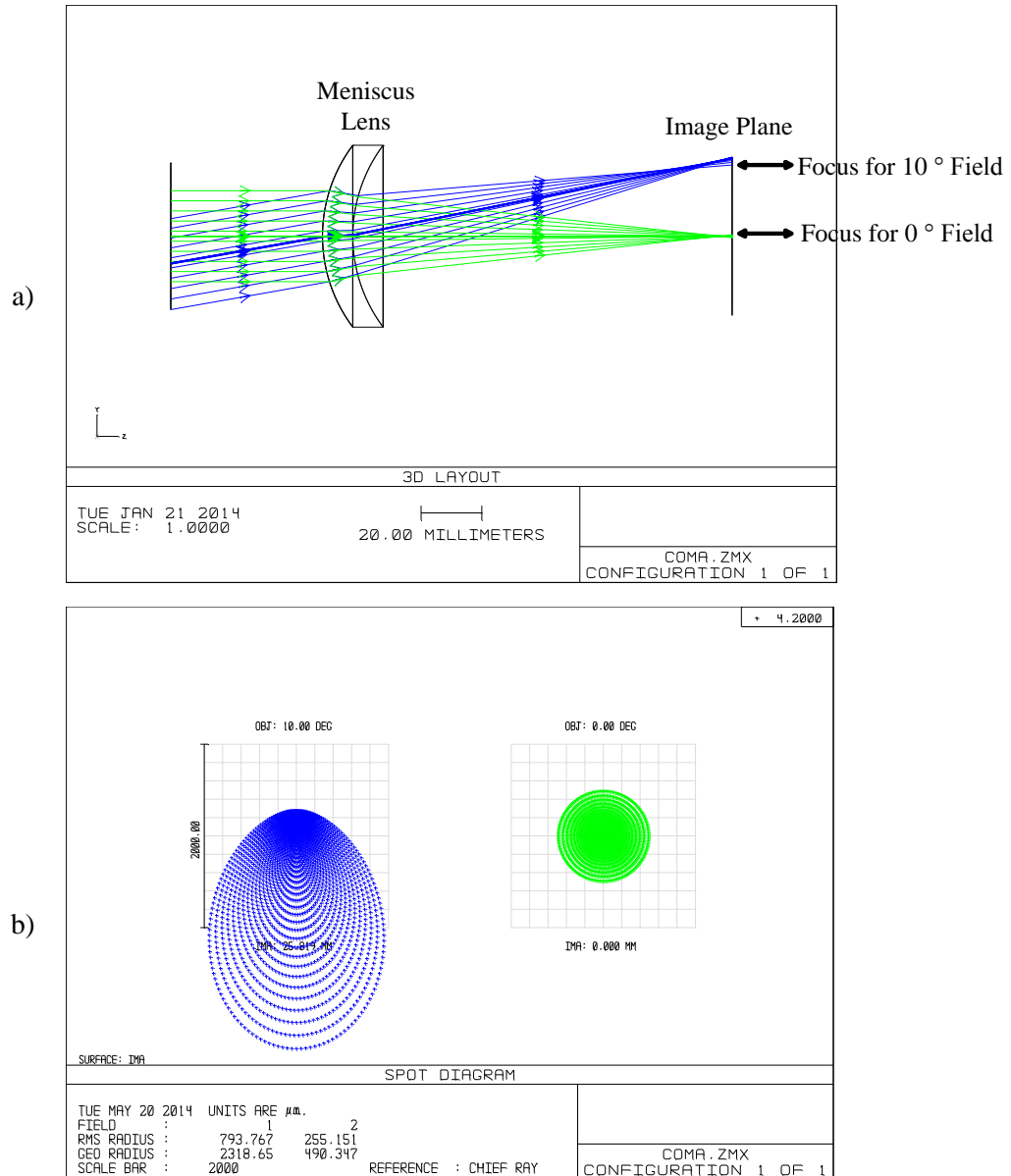
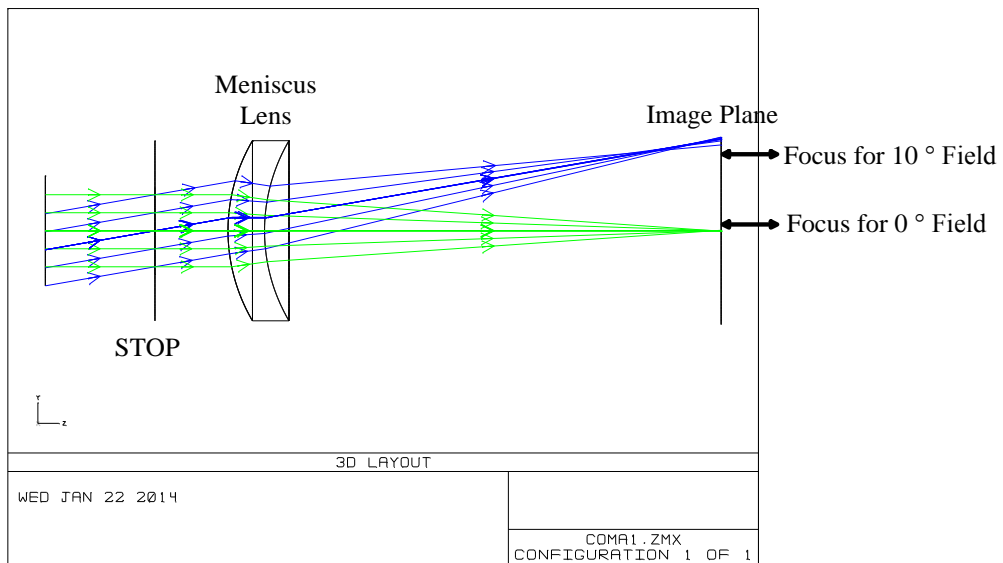


Figure 2.13 Optical aberration of a) coma, b) spot size of different fields.

As shown in Fig. 2.14 Coma can be reduced changing the aperture stop of the optical system.



a)

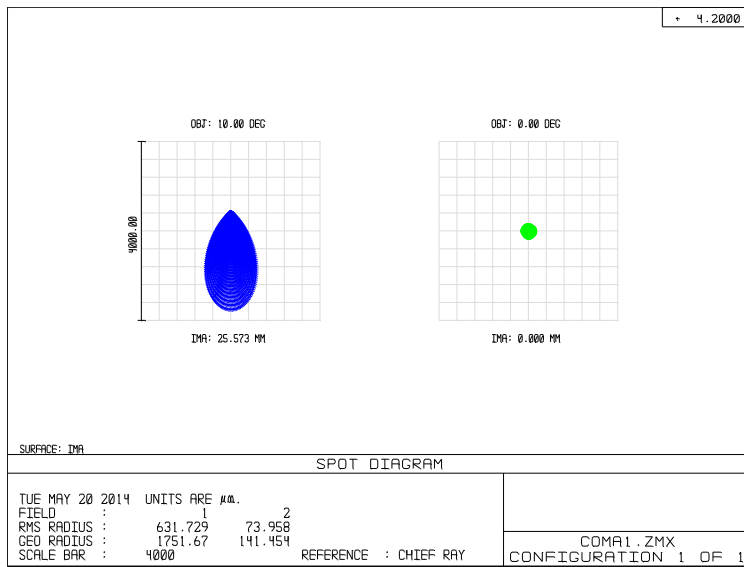
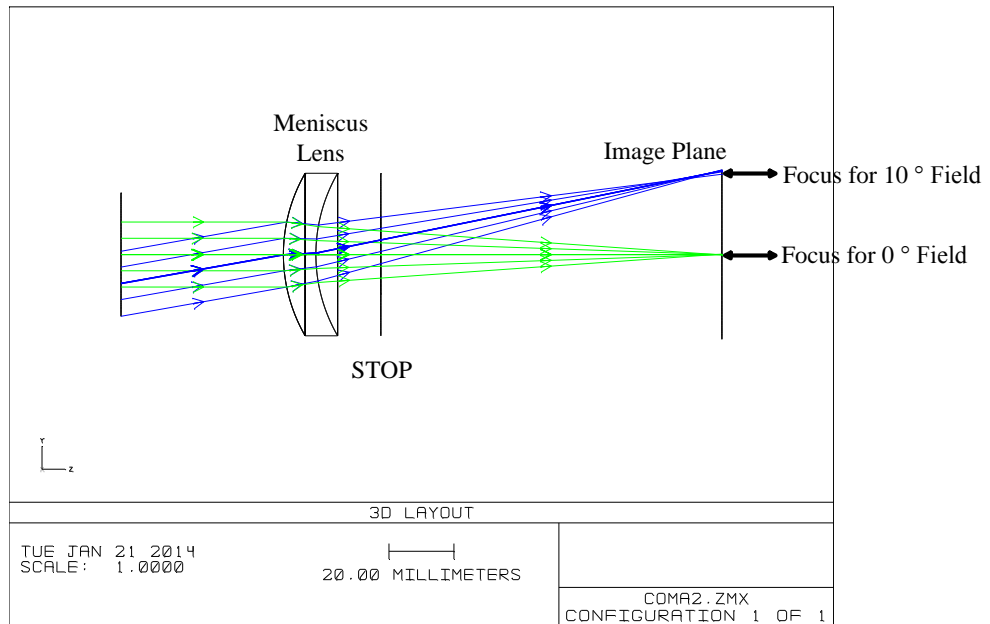


Figure 2.14 Different aperture stop positions are shown in a) coma with stop in front of lens, b) reduced coma with stop after lens



b)

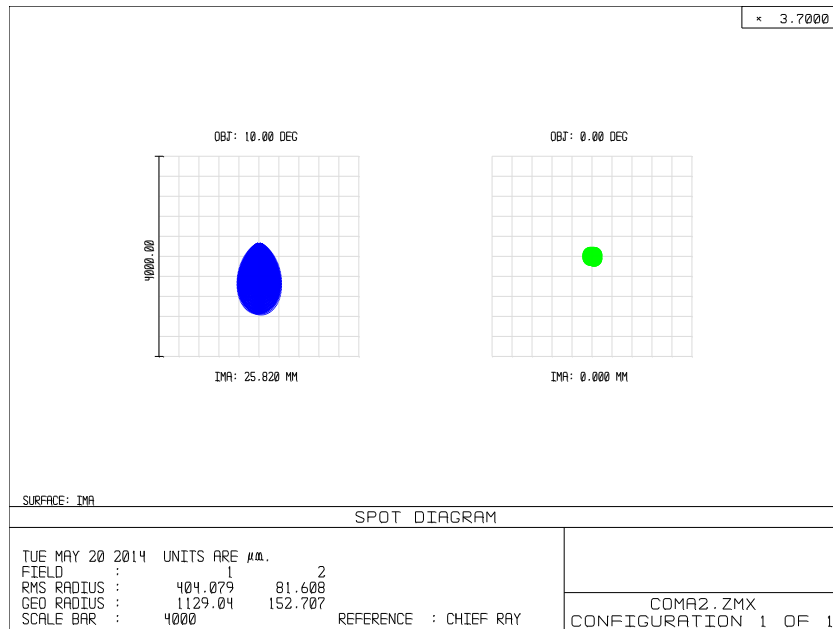


Figure 2.14 (continued)

Another optical aberration is called “*astigmatism*”. It causes from the rays in the meridional and sagittal planes are not focused at the same distance from the lens. Astigmatism is shown in Fig. 2.15 [15].

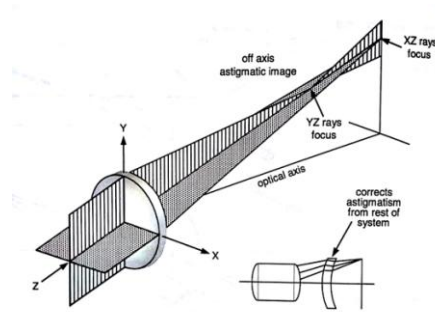


Figure 2.15 Astigmatism [15]

Another optical aberration is called “*field curvature*”. As shown is Fig. 2.16, focal plane is formed as a curve, not a plane. Reason for this aberration is that the back focal length changes with the field of the lens [15].

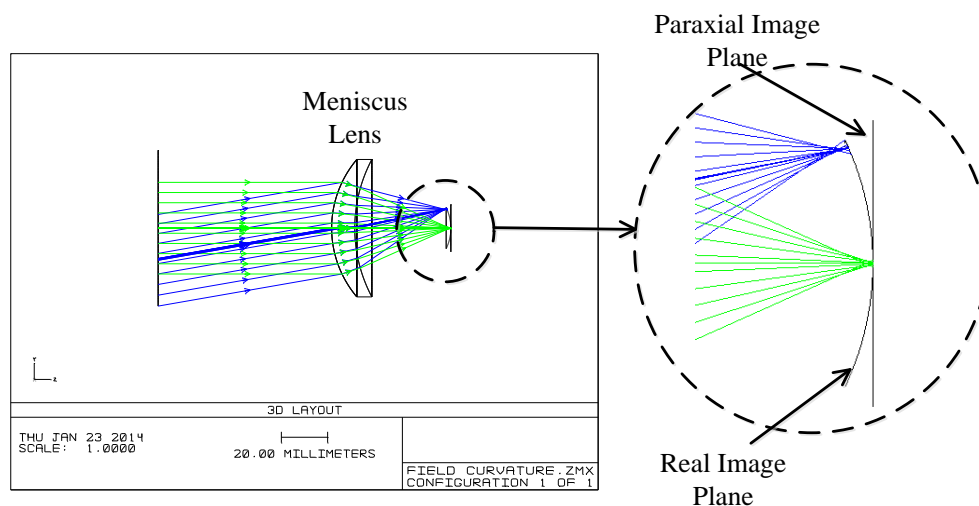


Figure 2.16 Field curvature

To reduce this aberration, there are two known methods. In first method, a negative lens is used between two positive lenses. Another method is to locate a negative lens near to the image plane [15].

Another optical aberration is called “*distortion*”. This aberration arises from the change of magnification because of the field of view or distortion effects overall

shape of the image. It causes depart from true replica of the object. For a good imaging system, the distortion should be less than 2% [1, 15]. Figure 2.17 shows different type of distortions. If the distortion dimension is greater than the detector dimension, the distortion is called positive distortion otherwise negative distortion.

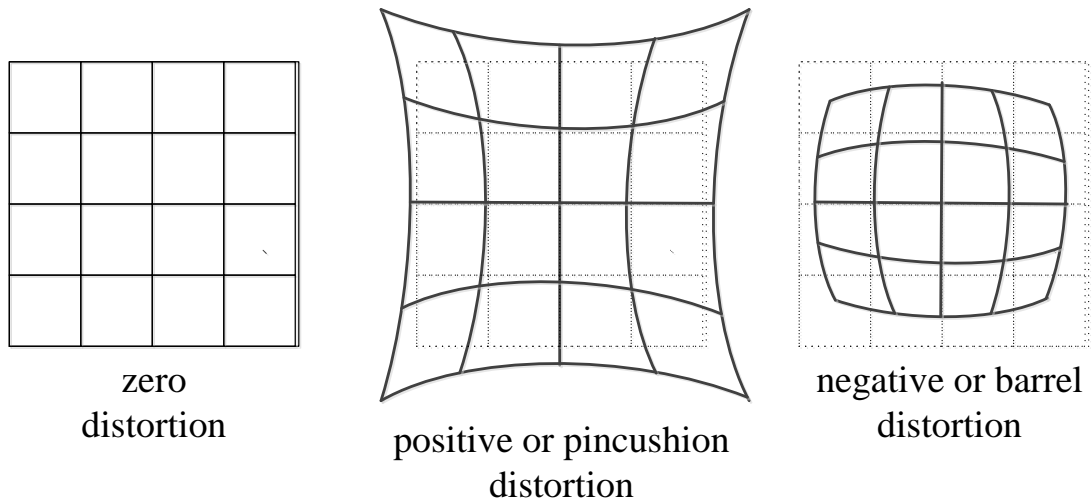


Figure 2.17 Distortion

Final aberration is called “*chromatic aberration*”. Refractive index is a function of wavelength. As a result, the focal length of the lens or effective focal length of the optical system will change with wavelength in axial direction and this is called “*longitudinal chromatic aberration*”. If the magnification changes in the lateral direction with wavelength, this is called “*lateral chromatic aberration*” [15]. These aberrations are shown in Fig. 2.18.

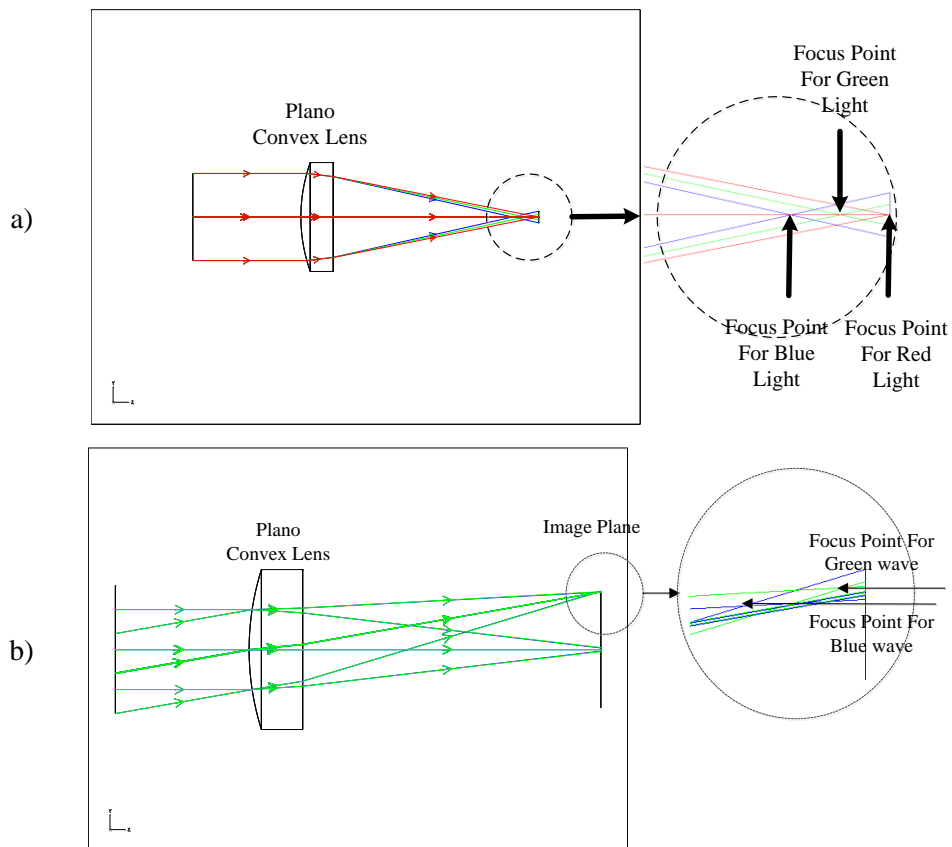


Figure 2.18 Chromatic aberrations a) Longitudinal chromatic aberration b) Lateral chromatic aberration

For an imaging optical system, OPD (optical path difference) is a method to measure the optical performance. As shown in Fig. 2.19, OPD is difference between the real wavefront and a spherical wavefront (ideal wavefront for perfect focus). The real wavefront departs from the spherical wavefront [15].

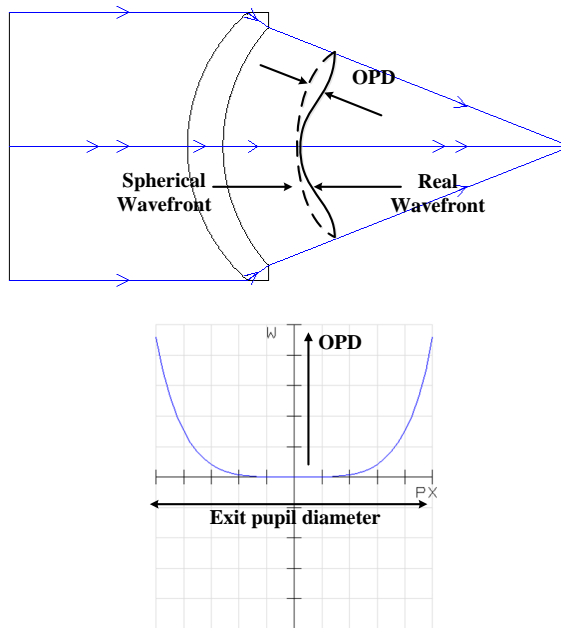


Figure 2.19 Optical path difference (OPD)

Lord Raleigh (real name is William Strutt, a Nobel Prize winner for discovering the gas argon) showed that [15]

*“An optical instrument would not fall seriously short of the performance possible with an absolutely perfect system if the distance between the longest and shortest paths leading to a selected focus did not exceed one-quarter of a wavelength.”*

As shown in Fig. 2.20, the image of a point source (which is known as a point-spread function) for different optical path differences cause different focuses. Note that the 0.25 wave OPD is nearly indistinguishable from the perfect airy disc [15].

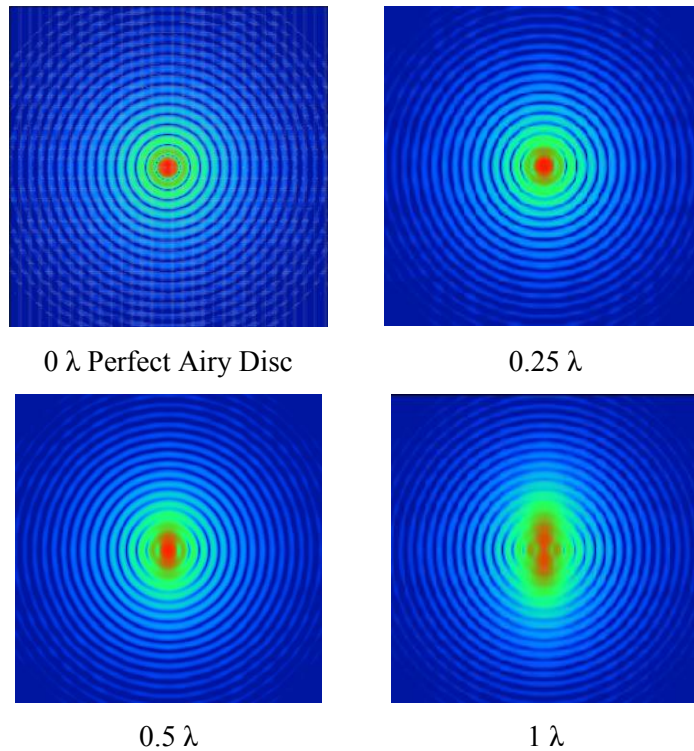


Figure 2.20 Image of a point source with different optical path difference due to coma

MTF is the most comprehensive of all optical system performance criteria, especially for image forming systems. The imagery will be degraded due to aberrations, assembly and alignment errors. MTF measures how the lens system transfers the modulation (or contrast) of the object to the image plane. Definition of MTF is

$$\text{Modulation} = \frac{I_{\max} - I_{\min}}{I_{\max} + I_{\min}} \quad (2.15)$$

where  $I_{\max}$  is the maximum intensity and  $I_{\min}$  is the minimum intensity. MTF shows how the object space is degraded in image plane after passing the optical system. Fig. 2.21 shows the object and image plane modulations.

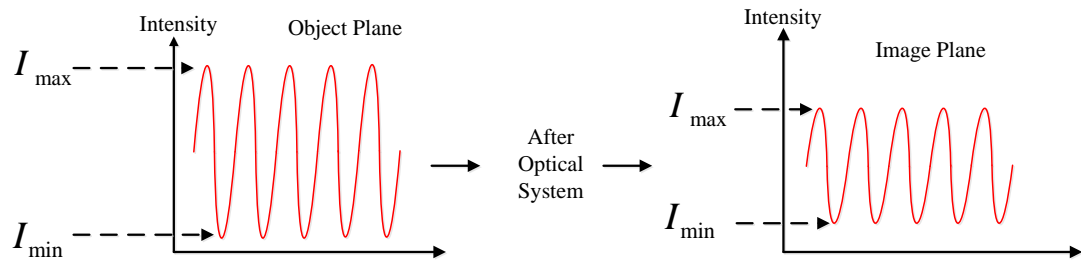


Figure 2.21 Meaning of the modulation transfer function

MTF is a function of spatial frequency and the cutoff frequency, which is where the MTF goes to zero, is

$$v_{cutoff} = \frac{1}{\lambda(f/\#)} \quad (2.16)$$

Fig. 2.22 shows a graphical representation of an object and of the resulting image at a low spatial frequency, a midspatial frequency and at high spatial frequency regions in spatial frequency domain [15].

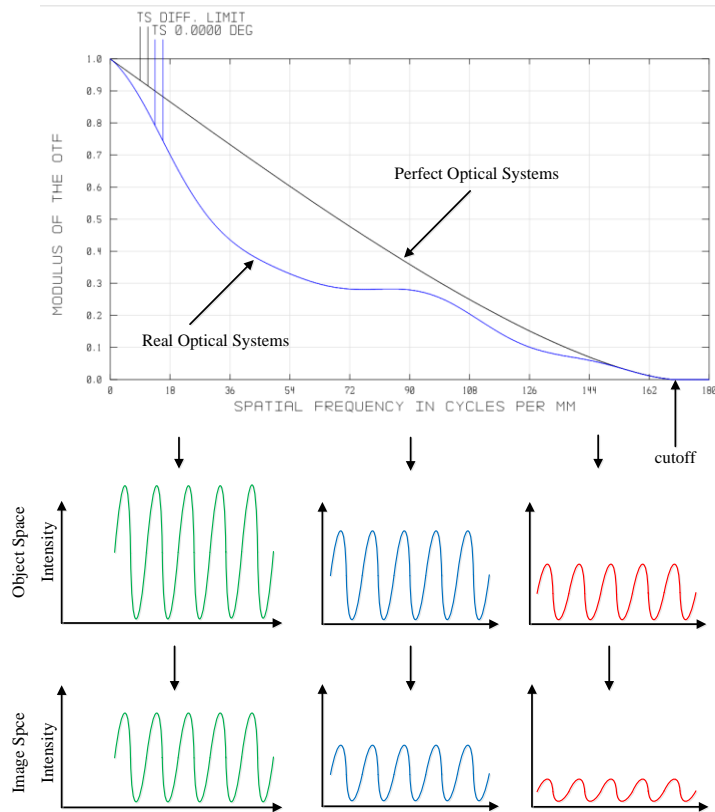


Figure 2.22 Typical MTF curves

## 2.6 Detector Parameters

In MWIR infrared band, QWIP (quantum well infrared photodetector) and Photoconductive type detectors are used mostly. These are all semiconductor based and are processed in clean room as a detector arrays and every detector element is called “*pixel pitch*”.

*NETD* (noise equivalent temperature difference) and  $D^*$  (Specific detectivity) parameters are mostly commonly used parameters that show the infrared detector performance.  $D^*$  is given as

$$D^* = \frac{A_d \sqrt{\Delta f}}{NEP} \quad (2.17)$$

where  $A_d$  is detector area and  $\Delta f$  is the noise bandwidth of the detector and NEP is the noise equivalent power which means that it is radiant flux to generate the signal to noise ratio is equal to 1.

Another detector parameter is NETD and it is given as

$$NETD = \frac{4F_{\#}^2 + 1}{\sqrt{A_p} \tau_{opt}} \frac{1}{\varepsilon \int_{\lambda_1}^{\lambda_2} \alpha(\lambda) \frac{\partial M_{\lambda, BB}}{\partial T} d\lambda} \frac{\sqrt{\Delta f}}{D^*} \quad (2.18)$$

$$NETD = \frac{4F_{\#}^2 + 1}{A_p \tau_{opt}} \frac{1}{\varepsilon \int_{\lambda_1}^{\lambda_2} \alpha(\lambda) \frac{\partial M_{\lambda, BB}}{\partial T} d\lambda} NEP \quad (2.19)$$

where  $F_{\#}$  is the F number of optical system,  $A_p$  is the detector pixel area,  $\tau$  is the transmission of optical system,  $\varepsilon$  is emissivity,  $\alpha(\lambda)$  is the absorption coefficient of detector,  $M_{\lambda, BB}$  spectral radiant exitance of blackbody and  $NEP$  is the noise equivalent power.  $NETD$  is generally measured at the 25 °C Blackbody and with no optics for MWIR detectors [5,19].



## CHAPTER 3

### DEVELOPMENT OF HEAT SEEKERS

Infrared homing is a passive missile guidance system that uses infrared emissions from aircraft to detect and lock on to the target. Missiles which use infrared seeking are called as "heat-seekers" and many aircrafts have been lost in warfare by heat seekers. Objects such as people, vehicle engines and aircraft emit heat as a radiation source and this radiation can be detectable by special detectors [10].

Radiations emitted from target and radiations emitted from background (sky) are in different temperatures (For air temperature is 22 °C and for Helicopter exhaust temperature is about 500 °C). This difference can be discriminated using optical systems and the angular position of the target can be determined by using temperature difference of the target from background. The entire heat seekers use this principle with their specific working mechanisms. Schematic representation of target, background and heat seeker are shown in Fig. 3.1.

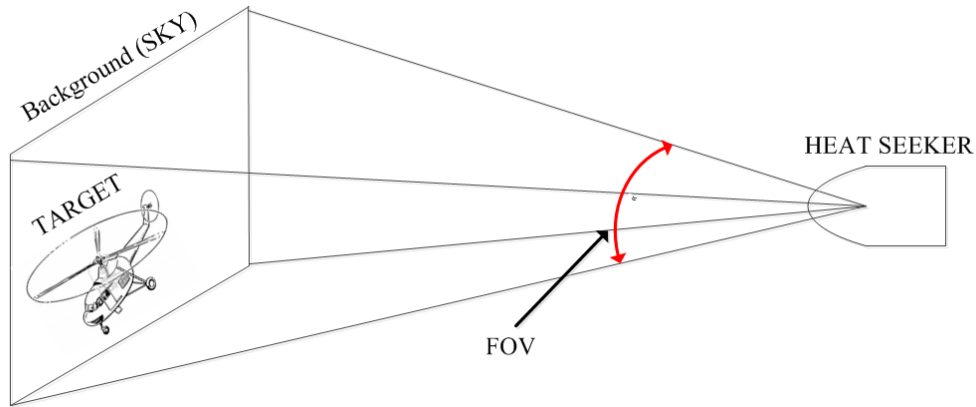


Figure 3.1 Schematic representation of a heat seeker and target (FOV; Field of view)

Heat-Seekers can be divided into two divisions as IR seekers and IIR (imaging infrared) seekers according to working mechanism how they find the angular position of target relative to the optical axis of heat seeker using temperature difference between target and background. And also they can be divided into more sub regions shown in the Fig. 3.2.

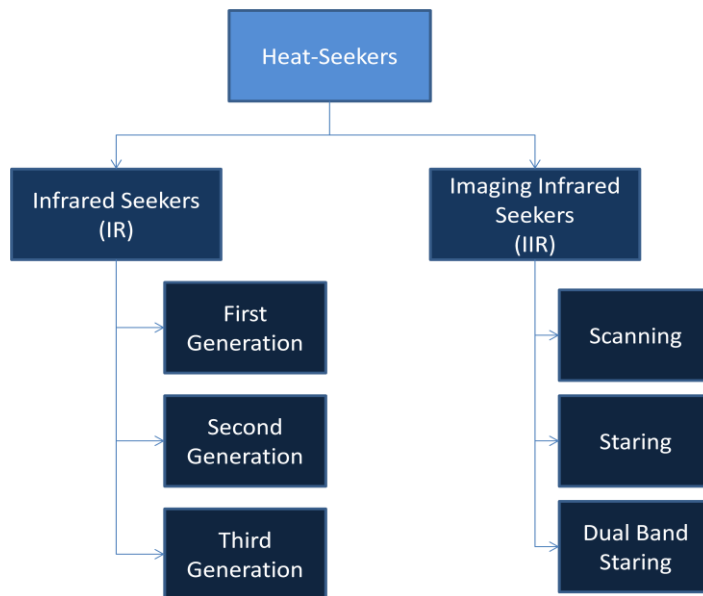


Figure 3.2 Heat seekers block diagram

### **3.1 Infrared Seekers**

Usually, IR seekers have single detector and they use a rotating “reticle” to detect the angular position of target. Optical system is used to collect and focus the infrared radiation from background and target onto the detector. Rotating reticle is used to modulate (Frequency, Amplitude) the infrared radiation on the detector. Infrared radiation of the background is less than the target radiation because of the temperature and it is uniform in all scenes, but target radiation is more powerful and comes to the optics on a specific angular position in scene. This difference is used to detect the angular position of the target.

The seekers using single detector have three types of scanning method: spin-scan, con-scan and rosette-scan. Infrared seekers can be divided into 3 sub regions according to their scanning methods or working principles [11].

#### **3.1.1 First Generation Infrared Seekers**

First generation infrared seekers have a reticle as shown in Fig. 3.3. The reticle has 3 different parts. One part is fully transparent shown on the Fig. 3.3 as white, one part is opaque shown on the Fig. 3.3 as black and the other part is semi transparent shown on the Fig. 3.3 as gray. When reticle is rotated, the power falling from the target onto the detector will change according to the rotating frequency and the reticle structure. The output of the detector according the rotation of the reticle is shown in Fig. 3.3 [11].

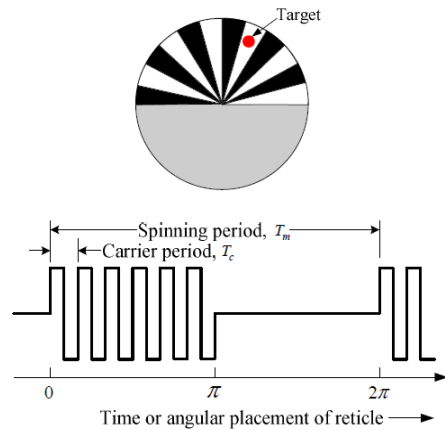


Figure 3.3 Reticle structure and the detector output pulse [11]

These types of seekers are also called spin-scan seekers. The optical structure of the spin-scan seeker is shown in the Fig. 3.4. There are four optical components, primary mirror, secondary mirror, reticle and detector. Primary and Secondary mirror is used to collect the radiation emitted from the target onto the detector and reticle is used to modulate (amplitude modulation) the infrared radiation. This type of modulation is also called Amplitude-Phase modulation.

Target signal and reference signal is compared while finding the angular position of target. When there is no target in the FOV of seeker the output of the detector is shown in Fig. 3.5 a). When there is a target in the FOV of the seeker, the output of the detector is shown in Fig. 3.5 b) and c). The difference in Fig. 3.5 b) and c) comes from the different angular positions of the target.

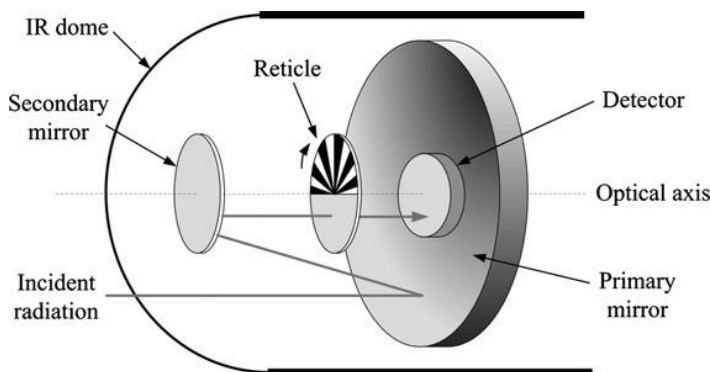


Figure 3.4 Optical structure of the 1. generation infrared seekers [12]

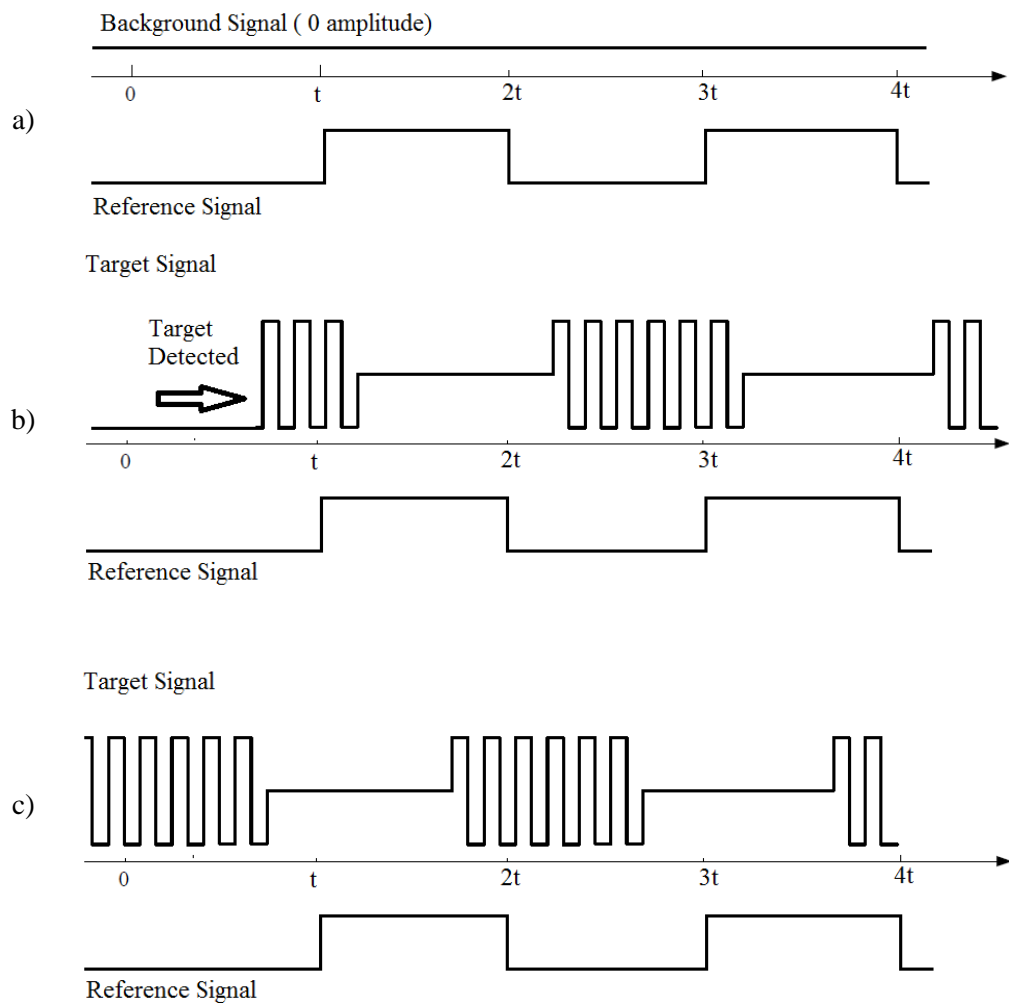


Figure 3.5 Time domain analysis a) no target, b) target, c) target in different angular position than case b).

### 3.1.2 Second Generation Infrared Seekers

Second generation seekers are called con-scan seekers. It is developed according to the drawbacks of the spin-scan seekers. When the target is on optical axes, in other words, the angle between seeker and the target is zero, spin scan seeker modulator does not work because the infrared radiation falls onto center of the reticle. Another drawback is semitransparent region of the reticle, the infrared radiation is lost %50. So, it directly affects the lock on range of the missile.

Con-scan seeker's optical structure is similar to the spin scan seekers. First difference is spin-scan seekers have stationary reticle and the structure shown in the Fig. 3.6 is combination of transparent and the opaque parts. Second difference is the secondary mirror is tilted and rotated instead of reticle. Due to tilted secondary mirror, the detector output signal of the modulated infrared radiation is shown in Fig. 3.6. This type modulation is also called Frequency-Phase modulation.

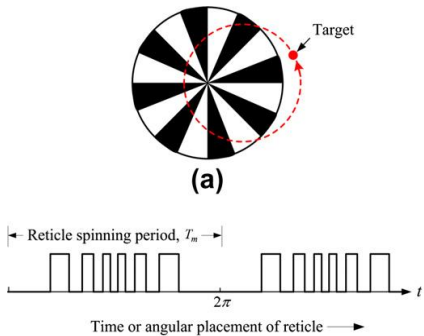


Figure 3.6 Structure and Its output of the con-scan reticle seeker [12]

### 3.1.3 Third Generation Infrared Seekers

Among the various IR seekers, the rosette scanning infrared seeker RSIS is a tracker in which a single detector scans the total field of view FOV in a rosette pattern. The rosette pattern is achieved by means of two counter-rotating optical elements such as prisms, tilted mirrors, or off centered lenses [13].

The optical structure of this type of missile is shown in Fig. 3.7. In this figure two wedges are counter-rotating. This provides the seeker rosette scanning property.

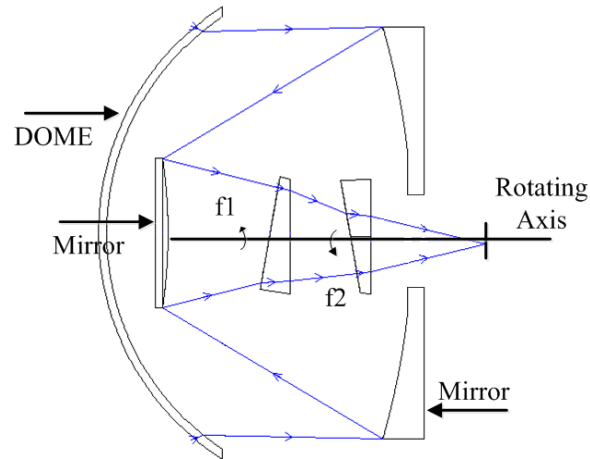


Figure 3.7 Optical structure of the rosette scanning infrared seeker ( $f_1$  and  $f_2$  rotating frequencies of prisms)

Working geometry of the rosette-scan missile is shown in Fig. 3.8.

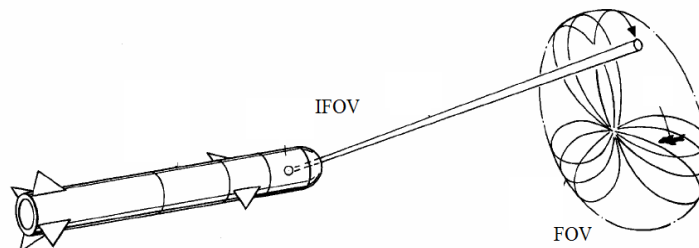


Figure 3.8 Working geometry of the rosette-scan seekers [14]

### 3.2 Imaging Infrared Seekers

Imaging infrared seekers are state of the art in infrared seeker technology. Because of the imaging nature of the system, small detector area (pixel of the detector), algorithms such as ATR (automatic target recognition) and ATA (automatic target acquisition) makes seeker more resistance to the countermeasures such as flares.

Imaging infrared seekers can be divided into 3 sub divisions due to working principles. Scanning infrared seekers has scanning component such as mirrors to

construct the image to the line element detector array. Staring seekers have no scanning optical component it uses a focal plane array to construct the image of the target. Dual band staring infrared seekers will be the future concept for the missile seekers. There is no such a seeker but it will be developed in the future because off-the-shelf products of dual band (MWIR and LWIR) FPAs can be found in detector company's catalogs.

**3.2.1 Scanning Infrared Seekers**

Scanning infrared seekers use line detector elements and try to construct the image of the scene using scanning mechanism with mirrors. Working principles are same with the IIR seekers. Only, the performance of the system depends on the scanning time of the mirrors. One of the scanning mechanisms of the scanning infrared seekers is shown in Fig. 2.32 and scanning infrared seekers can be subdivided into several subdivisions according to the scanning mechanisms. Dome is not shown in Fig. 3.9.

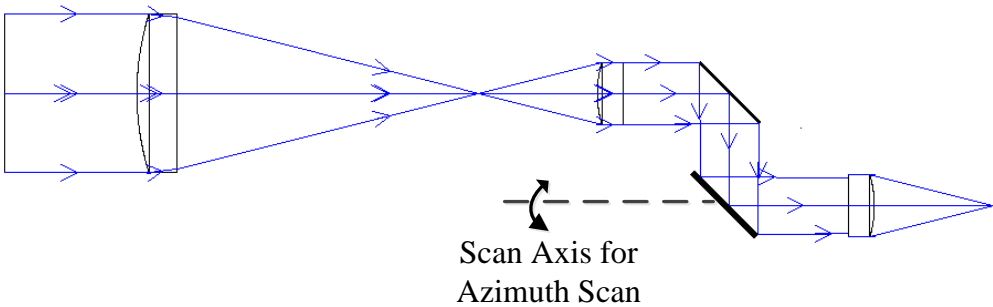


Figure 3.9 Schematic representation of scanning infrared seeker optic

Because of the scanning mechanism, working principle is complex as in the IR seekers. As in the IR seekers need and extra area in seeker for scan mirrors.

### 3.2.2 Staring Infrared Seekers

Nowadays, imaging infrared seekers are very popular in defense industry. Most of the missile seekers are using imaging infrared technology especially for aerial targets (MWIR) and for antitank missiles (LWIR).

IIR infrared seekers can easily counter to countermeasures such as flares. Because of the imaging nature of the system, target can be easily detected with algorithms such as (ATA; automatic target acquisition, ATR; automatic target recognition)

#### 3.2.2.1 Refractive Imaging Infrared Seeker

Optical representation of refractive imaging infrared seeker configuration is shown in Fig. 3.10. The configuration has 3 optical lenses (Positive meniscus, Biconcave and Positive Meniscus) and a focal plane array. Number of lenses and lens materials can be changeable according to the requirements of missiles such as FOV, focal length, weight etc. Dome is not shown in Fig. 3.10.

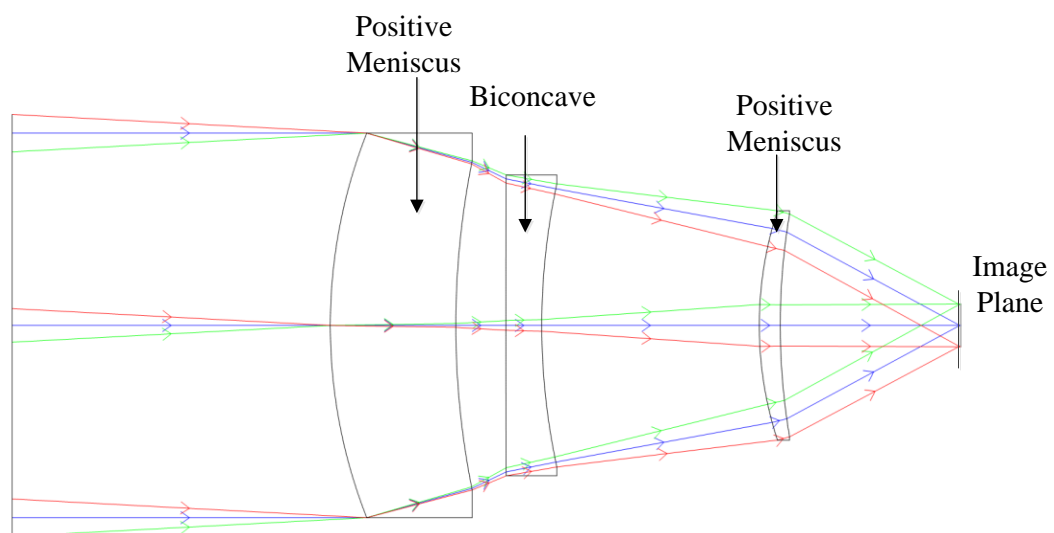


Figure 3.10 Optical representation of refractive imaging infrared seeker

### 3.2.2.2 Reflective Imaging Infrared Seeker

Optical configuration of reflective imaging infrared seeker is shown in Fig. 3.11. The configuration consists of mirrors to construct image of the scene onto the FPA. Mostly, Cassegrain optical configuration is used in such systems. In some optical systems corrector lens groups can be used with Cassegrain optical configuration. Dome is not shown in Fig. 3.11.

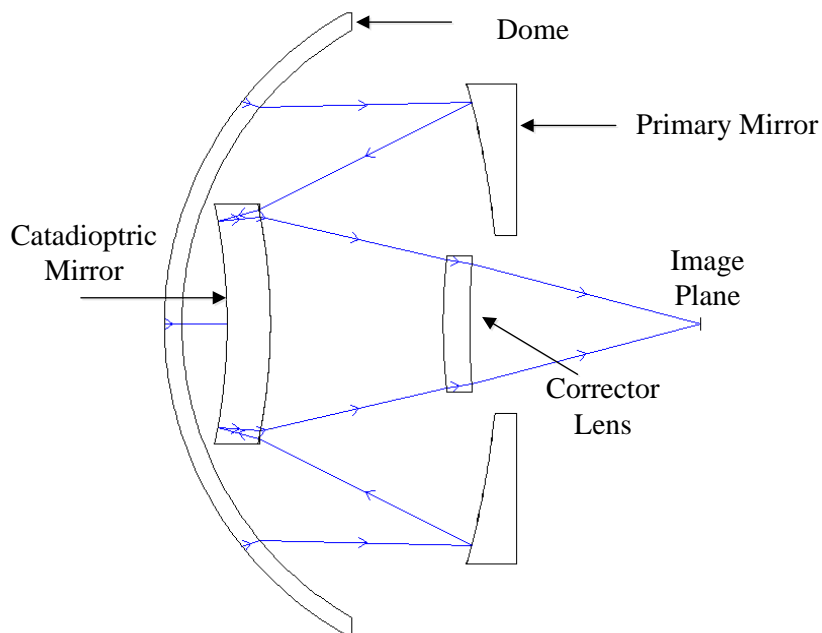


Figure 3.11 Optical representation of reflective imaging infrared seeker

### 3.2.3 Dual Band Staring Infrared Seekers

This is the future concept. Dual band infrared focal plane arrays or cameras are newly developed. The cost is much because of the technology of the detector elements. In near future the “Dual Band Staring Infrared Seekers” will be off-the-shelf products. Optical configuration may be classified into two sub categories but the spectrum of the band is very broad because it starts from  $3\mu\text{m}$  and ends with  $12\mu\text{m}$ . This makes the optical design very hard.

## CHAPTER 4

### SYSTEM DESIGN

#### 4.1 Detection Range Calculations

Detection range was taken as 5 km and target was chosen as an aircraft as shown in Fig. 2.7. The hot part of the aircraft is its nozzle and size of the nozzle was taken as  $5000 \text{ cm}^2$ . Temperature of the nozzle was considered as 750 K [9]. The seeker was designed for 140 mm diameter missile. This diameter may vary from missile to missile.

Before detection range calculations, spectral region must be determined. In Fig. 4.1 Spectral Radiant Exitance is plotted as a function of wavelength.

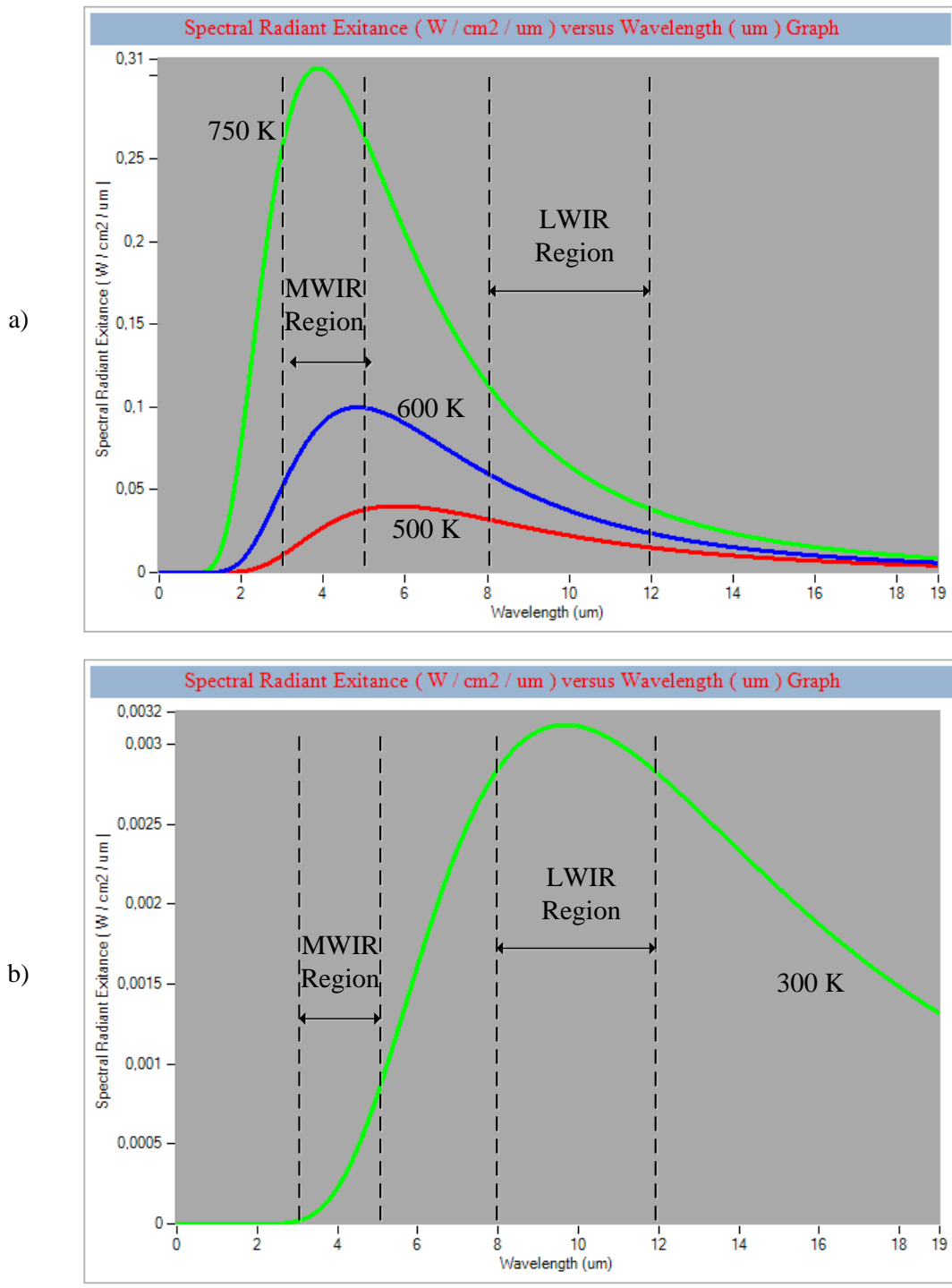


Figure 4.1 Spectral radiant exitance graph for a) 750 K, 600 K and 500 K objects, b) background 300 K object

MWIR region has much more thermal emission than the LWIR region. Although the nozzle of the aircraft radiates both in LWIR and MWIR regions, detection range is

longer in MWIR region because the radiation power is related with the temperature of the object. As shown in Fig. 4.1 a) MWIR region's spectral radiance is greater than the LWIR region. As a result, for high temperature objects, detection in long range applications, MWIR region should be used. If the target temperature was about 300 K, LWIR region would be used.

After spectral region was determined (by considering the object temperature), detector parameters were specified. Parameters are shown in Table 4.1

Table 4.1 Detector parameters [17]

Detector Type	InSb 2D Array
Array Format	320 x 256
Pixel Pitch	30 $\mu\text{m}$
NETD	20 mK
Cold Filter	3.6 $\mu\text{m}$ – 4.9 $\mu\text{m}$
Cold Shield	$F_{\#}=3$

In Table 4.1 detector type shows the detector material. Here, InSb material is used in detector to detect the infrared radiation. “*Array format*” shows the number of pixels. During this work 320 pixels are used in vertical direction and 256 pixels are used in horizontal direction. “*Pixel pitch*” shows the dimension of the pixel. The pixel pitch is 30  $\mu\text{m}$ . NETD is a measure of the detector sensitivity. It shows how sensitive is the detector. “*Cold filter*” shows the spectral region of the detector and it is a narrow window. The spectral region is between 3.6  $\mu\text{m}$  and 4.9  $\mu\text{m}$ . Radiation emitted from the aircraft was considered in this interval. “*Cold shield*” is used to cool the infrared detector. Schematic representation of the cold shield is shown in Fig. 4.2.

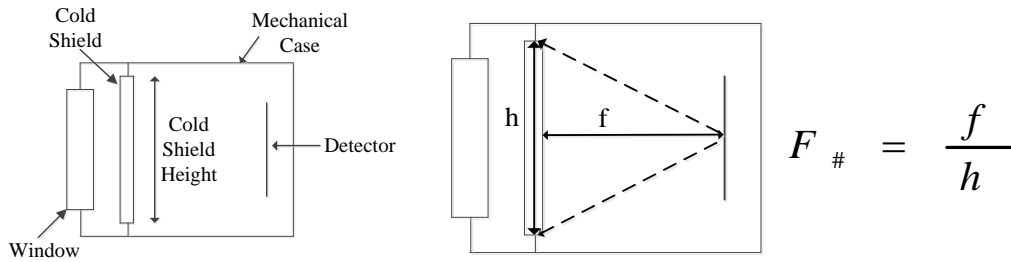


Figure 4.2 Cold shield and F/#

As shown Fig. 4.2, this configuration was used as a starting point for the seeker objective design. Also  $F_{\#}$  was given. To eliminate Narcissus effect, (Secondary and higher reflections between lenses cause some spots on focal plane array) all objective lenses are thought to have antireflection coatings instead of dome material. Dome material was selected as a sapphire material because it is durable to aerodynamic effects. Transmission of dome was taken approximately as 0.85 [21]. As a result total optical transmission was approximately 0.85, because lenses have antireflection coatings.

Fig. 4.3 shows interface of the software for infrared range calculation. This software was programmed in C# and developed codes were given in APPENDIX A. *NETD* is the figure of merit for IIR detectors. From *NETD*, detector noise (*NEP*) can be determined and according to results lock on range can be calculated for given optical parameters. Left column in Fig. 4.3, *NEP* was calculated. Calculation was done using “trapezoidal rule”. *NETD* is 20 mK, wavelength interval is between 4.9  $\mu\text{m}$  and 3,6  $\mu\text{m}$  spectral region (cold shield spectral region). Background temperature was taken as 295 K and emissivity was taken 0.98 [19], because MWIR sensors are tested at 22  $^{\circ}\text{C}$  temperature background conditions and with no optics. So, “T optics” (Transmission of optics) is equal to 1 and F number of optics is equal 1. Absorbance of detector was assumed as 0.6. (From literature, it is found that the reflectance of InSb material in MWIR region is approximately 0.40 [18]). Using Eq. 2.16, “*Infrared Range and NETD Calculator*” software was programmed. Interface is shown in Fig. 4.3.

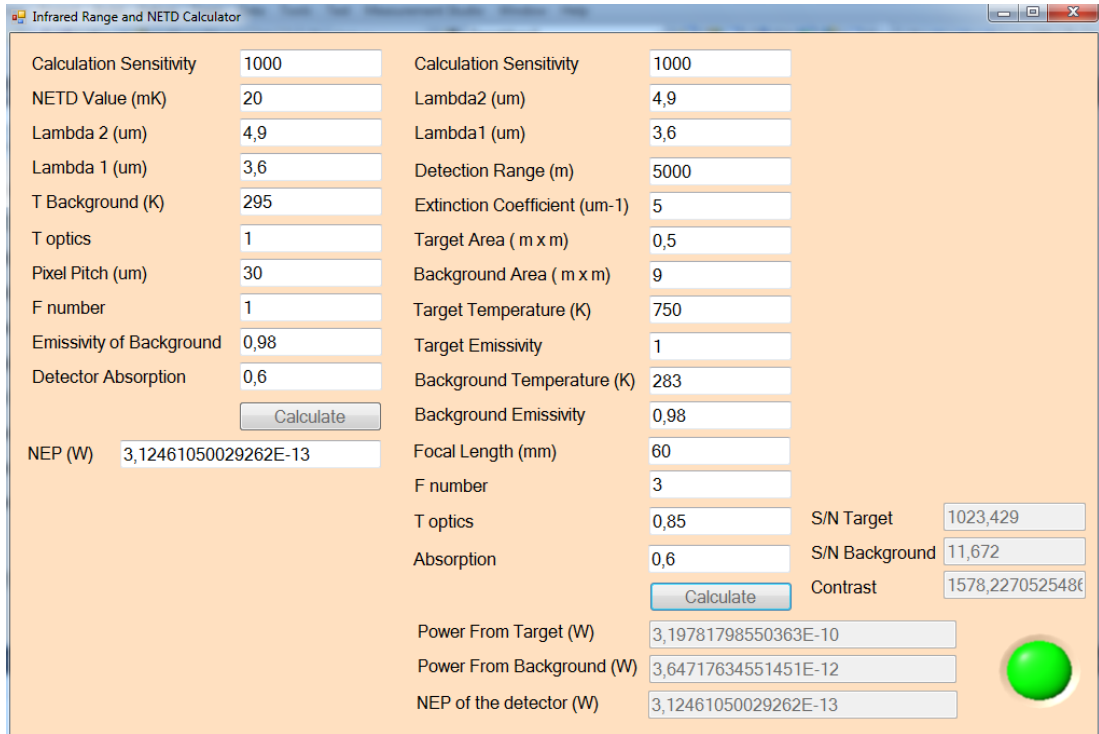


Figure 4.3 Infrared range and NETD calculator software interface

The  $NEP$  of detector is approximately  $3.12 \times 10^{-13}$  W. Signal comes from the target must greater than the noise of detector and the background radiation.

For detection range calculation, right column was used which is shown in Fig. 4.3. For lock on range condition, power from target must be greater than power from background and also  $NEP$  of detector.

$$P_{\text{target}} = \left( \varepsilon_{\text{target}} \frac{1}{\pi} \int_{\lambda_1}^{\lambda_2} M_{\lambda} d\lambda \right) \cdot A_{\text{target}} \cdot T_{\text{atm}} \cdot T_{\text{opt}} \cdot \Omega_{\text{target}}$$

$$P_{\text{background}} = \left( \varepsilon_{\text{background}} \frac{1}{\pi} \int_{\lambda_1}^{\lambda_2} M_{\lambda} d\lambda \right) \cdot A_{\text{background}} \cdot T_{\text{atm}} \cdot T_{\text{opt}} \cdot \Omega_{\text{background}}$$

where  $A$  is area of target and background,  $T_{atm}$  is the transmission of atmosphere,  $T_{opt}$  is transmission of optic,  $\varepsilon$  is the emissivity,  $M_\lambda$  is the spectral radiant exitance in interval between  $\lambda_1$  and  $\lambda_2$  and  $\Omega$  is the solid angle seen by optics.

Wavelength interval was taken according to cold shield properties (between 3.6  $\mu\text{m}$  and 4.9  $\mu\text{m}$ ).  $F_\#$  is a detector property and was taken as 3.  $A_{\text{target}}$  was taken as 5000  $\text{cm}^2$  and  $A_{\text{background}}$  was calculated using the geometry for single pixel as shown in Fig. 4.4;

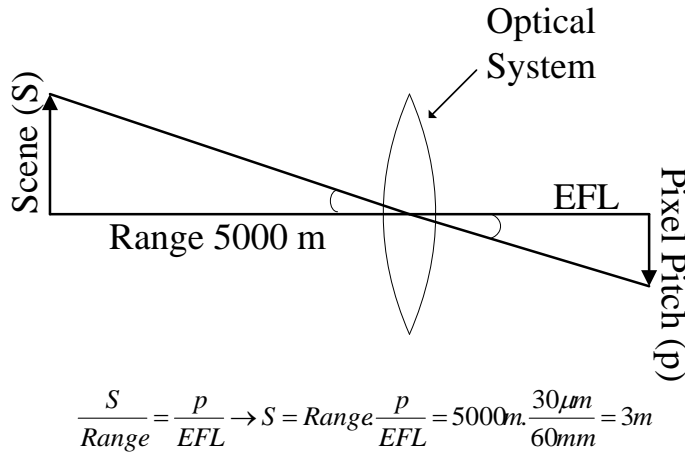


Figure 4.4 Background dimension calculation

where  $A_{\text{background}} = (3\text{m})^2 = 9\text{m}^2$ . Fig. 4.5 shows solid angle ( $\Omega$ ) calculations. For background and target, same solid angle was used because target and background were assumed as a point source.

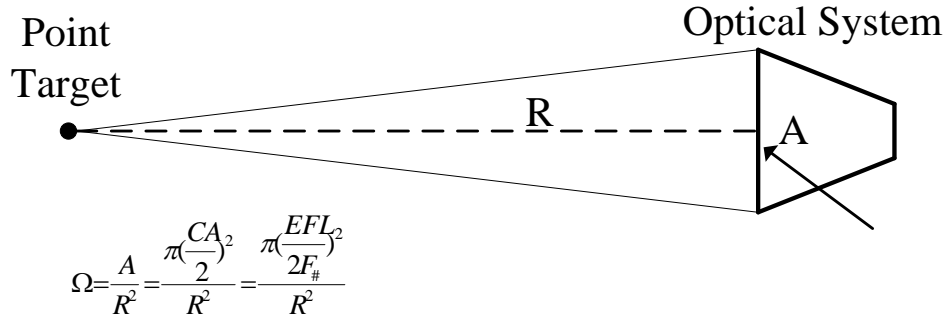


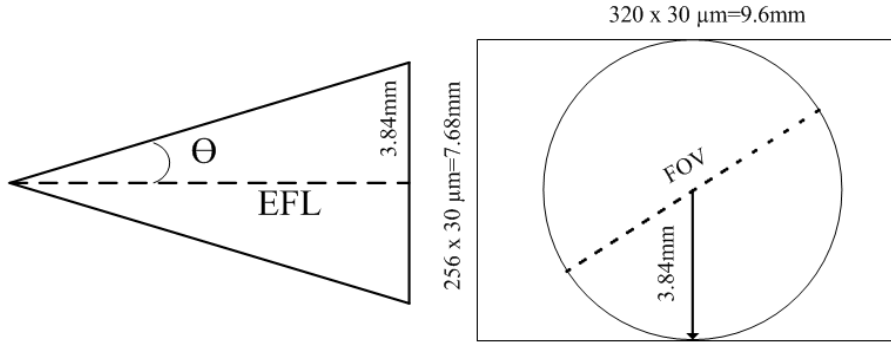
Figure 4.5 Solid angle calculations.

Transmission of atmosphere was calculated using Eq. 2.1 and extinction coefficient  $\sigma$  was taken as  $5 \times 10^{-6} \text{ cm}^{-1}$  [20].

Focal length of the optical system was determined under those situations. Focal length of the system is  $60 \text{ mm}$ .  $P_{\text{target}}$ ,  $P_{\text{background}}$  and  $NEP$  of detector were calculated as  $3.198 \times 10^{-10} \text{ W}$ ,  $3.647 \times 10^{-12} \text{ W}$  and is  $3.12 \times 10^{-13} \text{ W}$ . Power from background and  $NEP$  values are below the target radiation. As a result detection can be provided.

## 4.2 Optical Design of Seeker Objective

The spectral region of the optical system is between  $3.6 \mu\text{m}$  and  $4.9 \mu\text{m}$ .  $F_{\#}$  is 3 and effective focal length was calculated as  $60 \text{ mm}$ . Fig. 4.6 shows FOV calculation for the optical system.



$$\tan \theta = \frac{3.84\text{mm}}{EFL} = \frac{3.84\text{mm}}{60\text{mm}} \Rightarrow FOV = \pm\theta = \pm \tan^{-1}\left(\frac{3.84}{60}\right) = \pm 3.66^\circ$$

Figure 4.6 FOV calculation for optical system

FOV can be taken as  $\pm 3.7^\circ$  approximately. Optical parameters were summarized in Table 4.2.

Table 4.2 Optical parameters

Spectral Region	3.6 $\mu\text{m}$ -4.9 $\mu\text{m}$
EFL	60 mm
F <sub>#</sub>	3
FOV	$\pm 3.7^\circ$
Optical Transmission	0.85

Required effective focal length is 60 mm, diffraction limited spot diameter for 3.6  $\mu\text{m}$  wavelength is 26.4  $\mu\text{m}$  and for 4.9  $\mu\text{m}$  wavelength 29.3  $\mu\text{m}$ .

Lens parameters were calculated from Eq. 2.14. and Eq. 2.12, second surface of the lens with desired effective focal length was derived. The derivation was

$$R_2 = \left( \frac{(n-1)[2(n+2)EFL - (2n+1)CT]}{n(2n+1) - 2(n+2)} \right) \quad (4.1)$$

Using Eq. 4.1 and Eq. 2.14 with 8 mm *CT* of the single sapphire (refractive index was taken as 1.7 [23]) lens parameters were calculated. Lens parameters are shown in Table 4.3. Zemax simulation results are shown in Fig. 4.13 a) shows optical system configuration and Fig. 4.13 b) shows spot sizes for different fields such as  $0^\circ$ ,  $\pm 3.7^\circ$ , etc.

Distance between Lens1's second surface and Stop point is 39.506 mm. Total length of the optical system is 66.906 mm.

Table 4.3 Lens parameters for case 1

	Material	CT (mm)	R1 (mm)	R2 (mm)	Conic Constant
Lens1	Sapphire	8	43.35	646.19	0
BFL	-	58.906	-	-	-

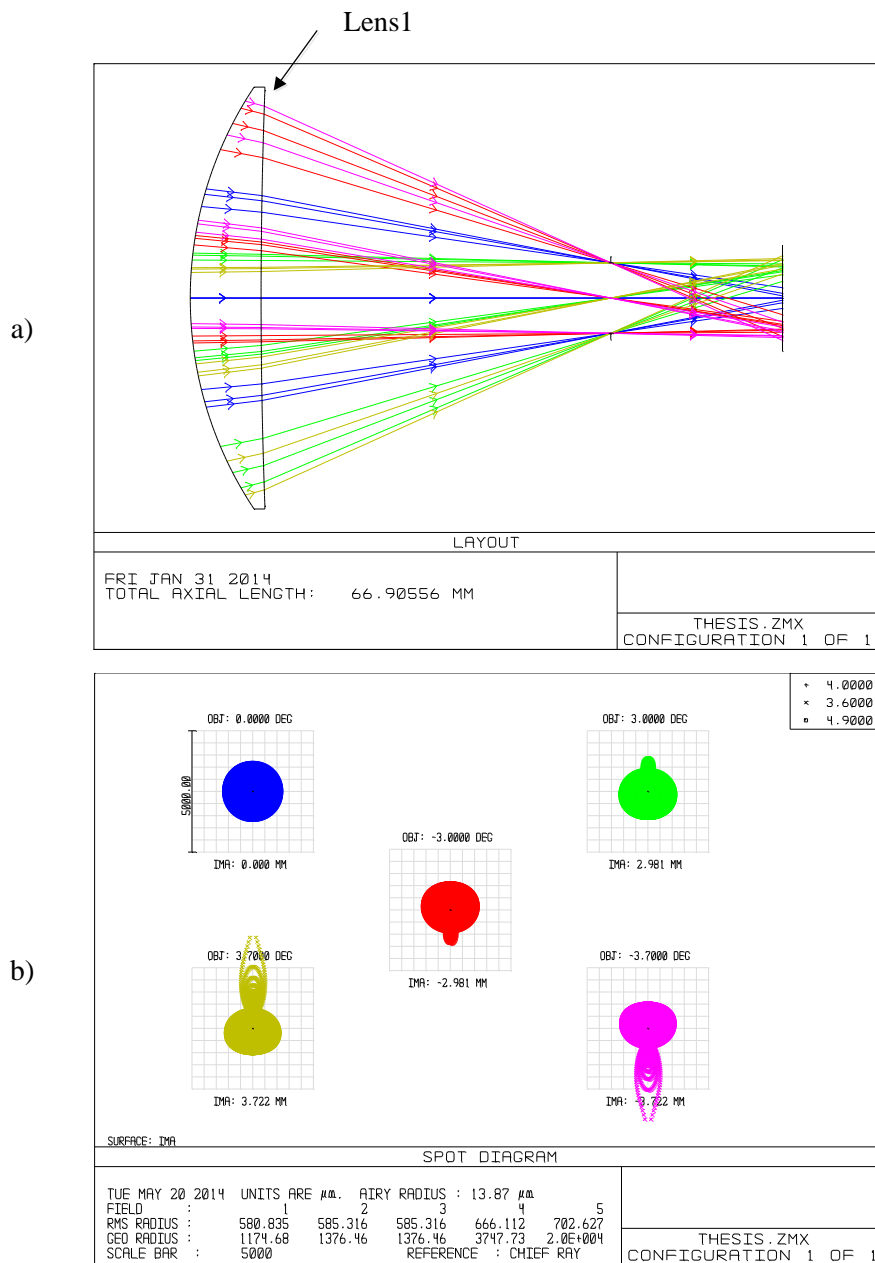


Figure 4.7 Zemax simulations for case 1; a) optical system, b) spot sizes for different fields.

As shown in Fig. 4.7 spot diameter of single lens was found approximately 5 mm and effective focal length of the system was found 68.45 mm. Required spot diameter is below 30  $\mu\text{m}$  and effective focal length is 60 mm.

First surface, second surface and BFL were optimized to desired effective focal length and spot sizes. Results are shown in Fig. 4.8 and Table 4.4.

As shown in Fig. 4.8, effective focal length was reached to desired value (60 mm). Although the spot size was reduced to approximately 4 mm, it is not in desired dimensions. Parameters were shown in Table 4.4.

Table 4.4 Lens parameters for case 2

	Material	CT (mm)	R1 (mm)	R2 (mm)	Conic Constant
Lens1	Sapphire	8	33.061	162.430	0
BFL	-	51.209	-	-	-

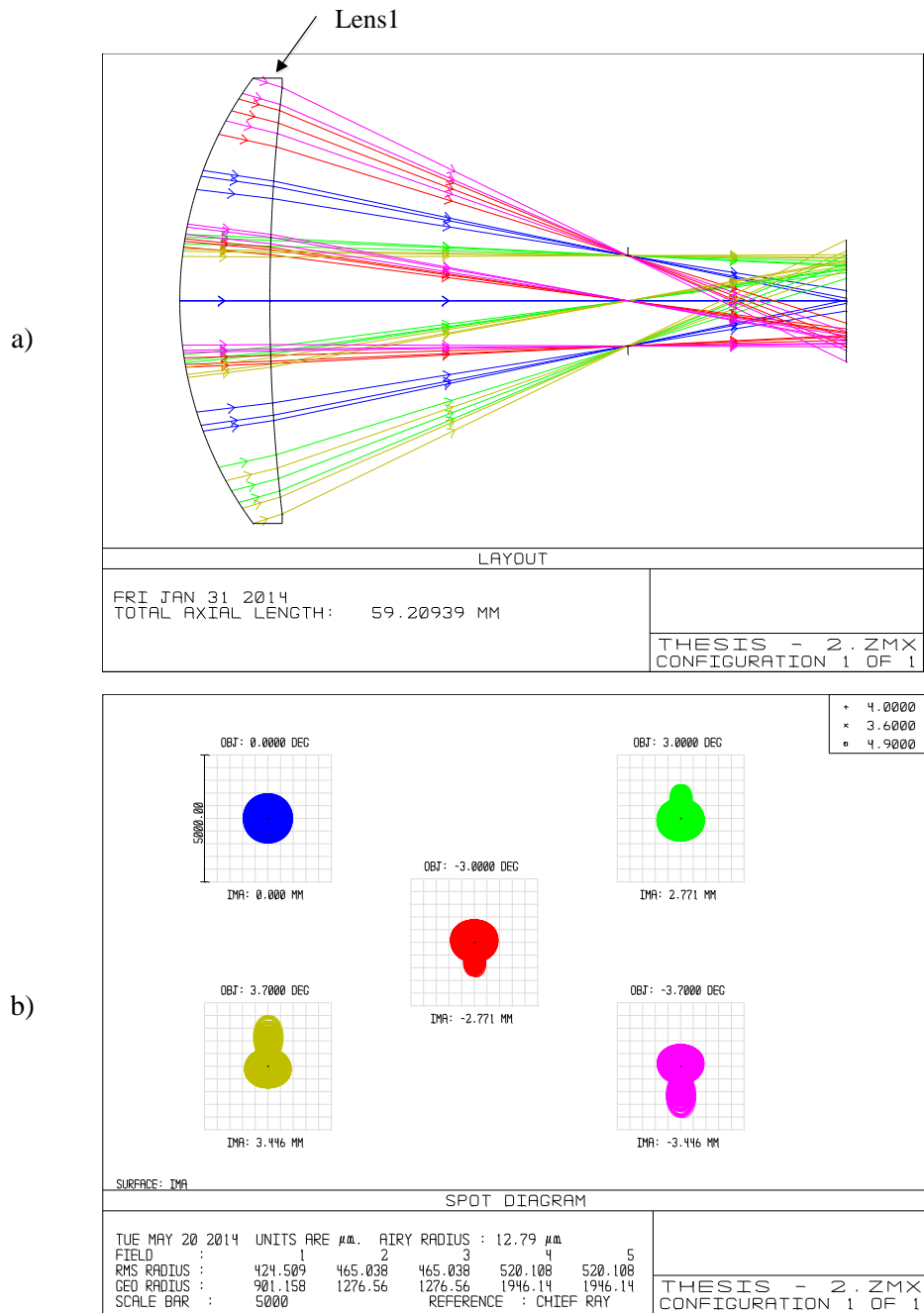


Figure 4.8 Zemax simulations for case 2; a) optical system, b) spot sizes for different fields.

To reach required values of spot size, single sapphire lens was splitted into two lenses. First surface of Lens1, second surface of Lens2 and First surface's conic constant of Lens1 were chosen as variable and optimized using Zemax's

optimization tool. Optical system and spot sizes for different fields are shown in Fig. 4.9. Lens parameters are given in Table 4.5.

Table 4.5 Lens parameters for case 3

	Material	CT (mm)	R1 (mm)	R2 (mm)	Conic Constant
Lens1	Sapphire	8	33.061	infinity	-0.360 First Surface
Air	-	4	-	-	-
Lens2	Sapphire	4	infinity	52.620	0
BFL	-	42.4	-	-	-

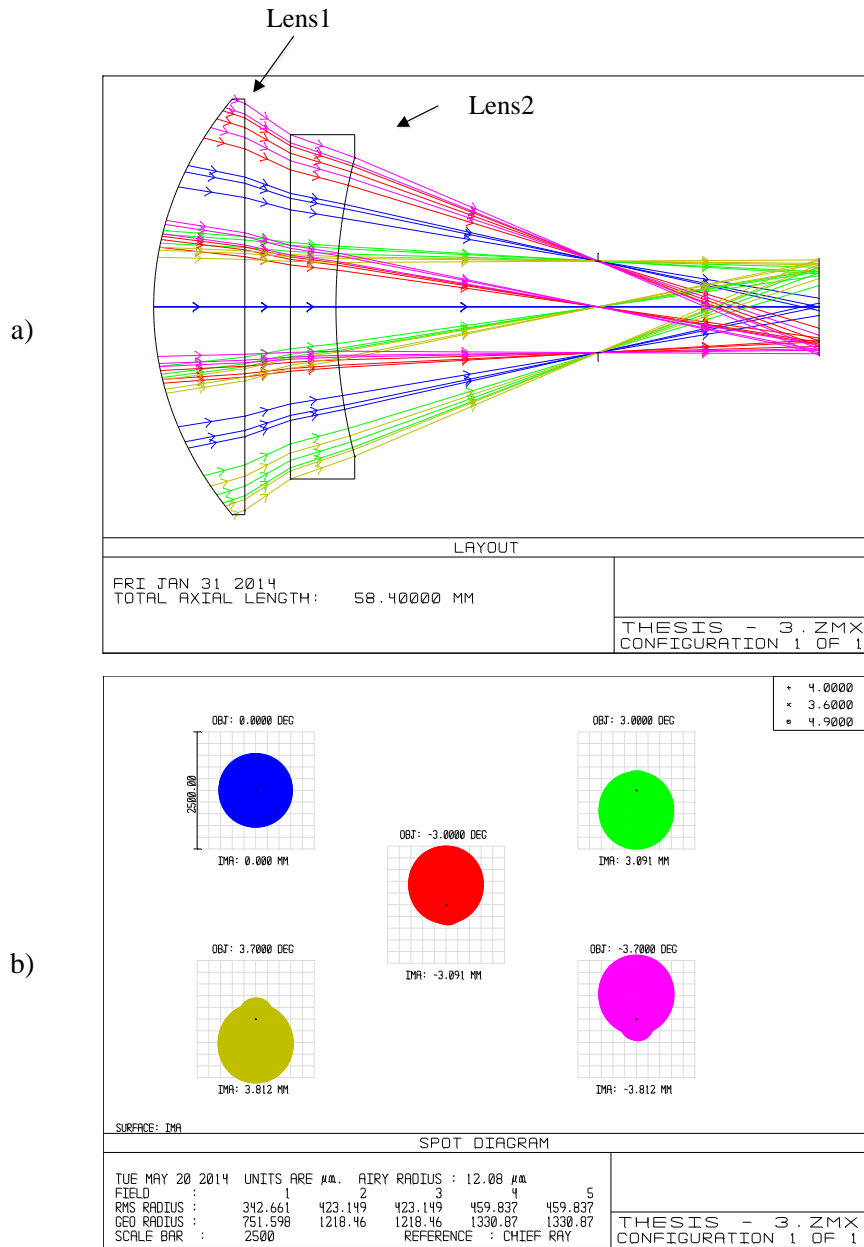


Figure 4.9 Zemax simulations for case 3; a) optical system, b) spot sizes for different fields.

As shown in Fig. 4.9, spot sizes were found about 2 mm diameter. So it is not in desired values. Using Hammer Optimization, optimization was done for Lens1 and Lens2. First and second surface of Lens1, first and second surface of Lens2, CT of Lens1 and Lens2, BFL and first surface's conic constant were chosen as variable.

Optimized optical system is shown in Fig. 4.10 and lens parameters are given in Table 4.6.

Table 4.6 Lens parameters for case 4

	Material	CT (mm)	R1 (mm)	R2 (mm)	Conic Constant
Lens1	Sapphire	2	39.945	37.445	-0.135 First Surface
Air	-	4	-	-	-
Lens2	GaAs	3	41.798	36.473	0
BFL	-	55.873	-	-	-

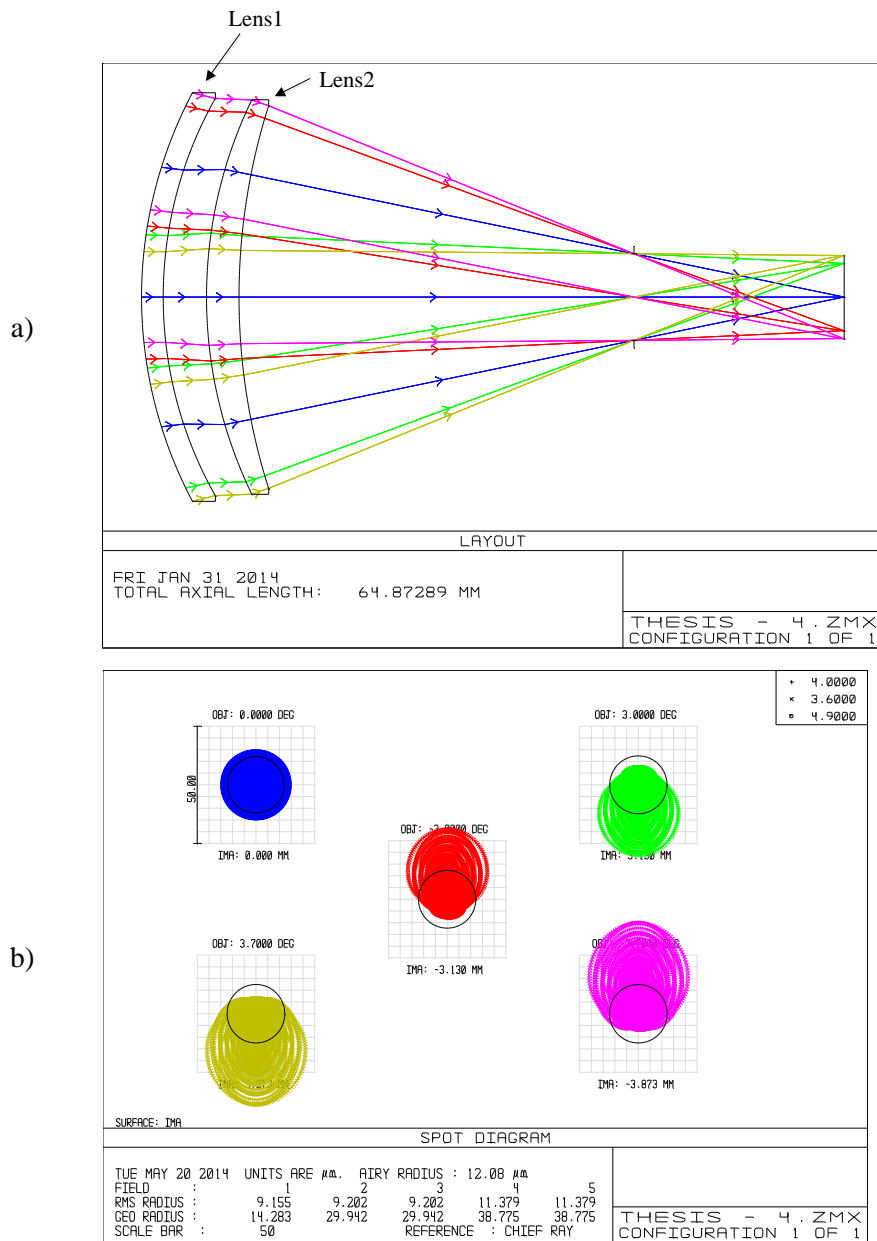


Figure 4.10 Zemax simulations for case 4; a) optical system, b) spot sizes for different fields.

As shown in Fig. 4.10 spot sizes of the optical system are reached to desired values. Approximately they are about 50  $\mu\text{m}$ . To reach desired values distance between lenses, BFL, all radiuses of the lenses and first surface's conic constant of Lens1 were chosen as variable and Hammer optimization was done. Results are shown in Fig. 4.11 and Table 4.7.

Table 4.7 Lens parameters for case 5

	Material	CT (mm)	R1 (mm)	R2 (mm)	Conic Constant
Lens1	ZNS_BROAD	3	48.200	34.552	-0.054 First Surface
Air	-	1	-	-	-
Lens2	SILICON	3	35.699	55.322	0
BFL	-	55.27	-	-	-

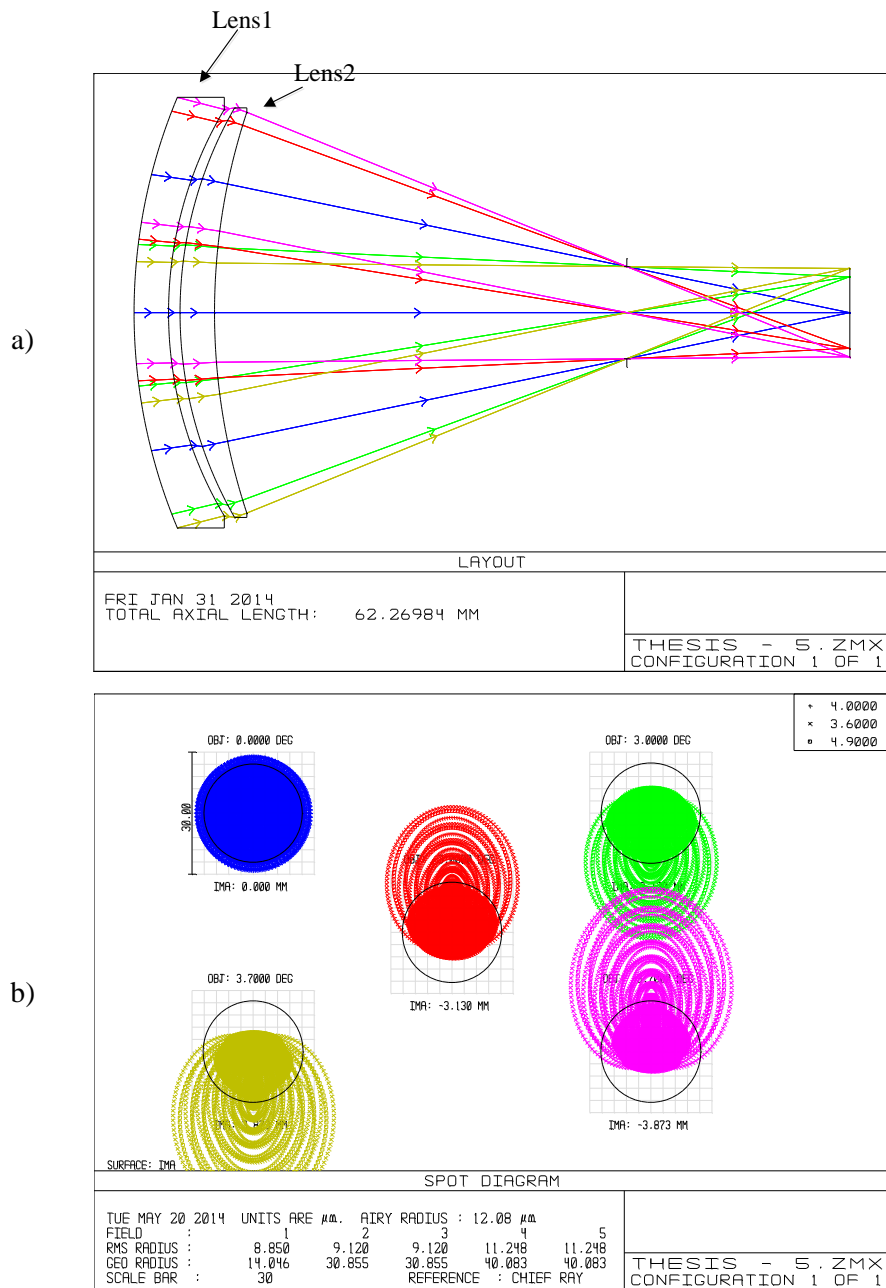


Figure 4.11 Zemax simulations for case 5; a) optical system, b) spot sizes for different fields.

As shown Fig. 4.11 b) spot radius of the field zero is below  $30 \mu\text{m}$  but other fields are greater than  $30 \mu\text{m}$ . Optical system has coma aberration as shown in Fig. 4.11 spot sizes. In MWIR systems, spot positions are constant and an extra lens must be added to the system to get rid of the coma aberration.

To reach desired values, distances between lenses, BFL, all radiuses of the lenses, all CT of lenses, second surface's conic constant of Lens2 and first surface's conic constant of Lens3 were chosen as variable and Hammer optimization was done. Results are shown in Fig. 4.12 and Table 4.8.

Table 4.8 Lens parameters for case 6

	Material	CT (mm)	R1 (mm)	R2 (mm)	Conic Constant
Lens1	GE_OLD	2.822	39.528	31.783	0
Air	-	2	-	-	-
Lens2	SILICON	4.042	34.352	53.759	0.043 Second Surface
Air	-	36.15	-	-	-
Lens3	CDSE	3.583	49.178	56.378	-5.833 First Surface
BFL	-	21.4	-	-	-

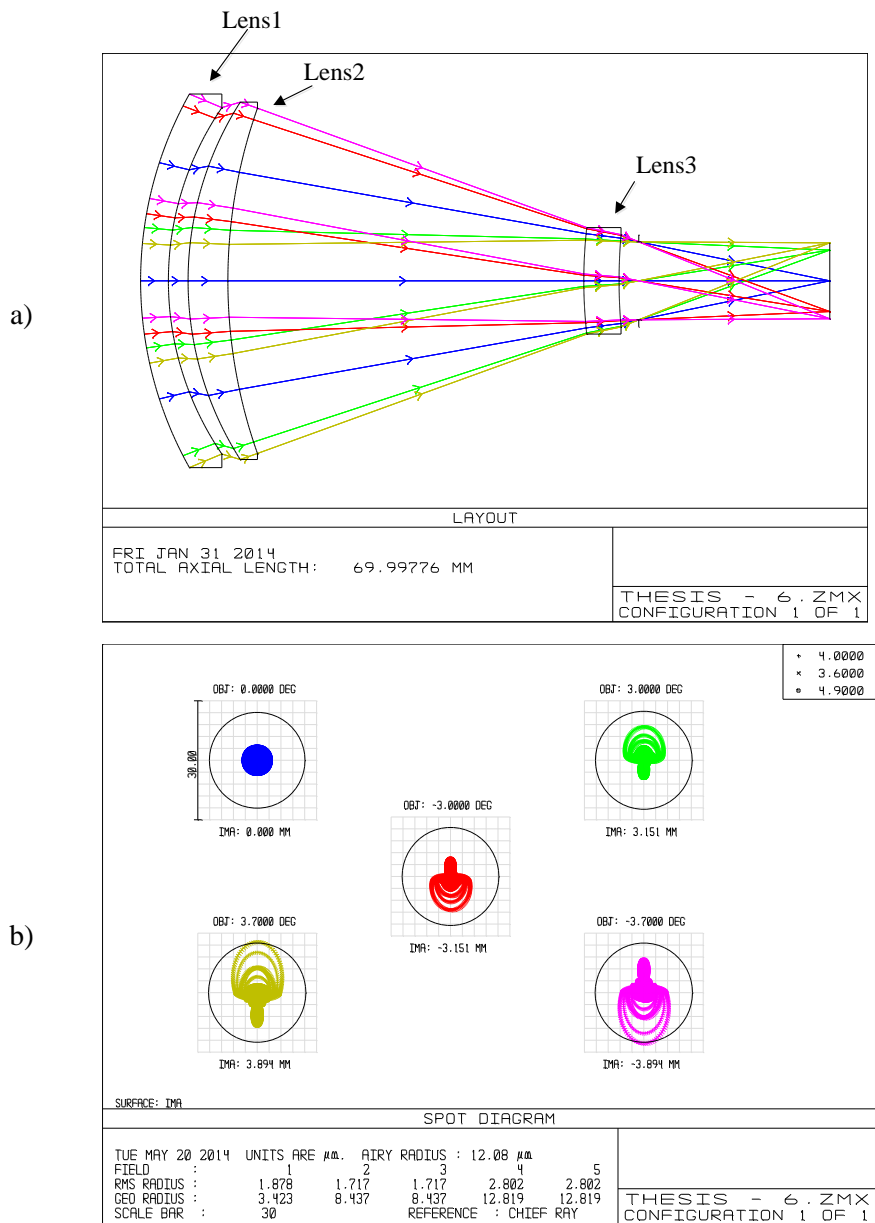


Figure 4.12 Zemax simulations for case 6 ; a) optical system, b) spot sizes for different fields.

As shown Fig. 4.12 b) all spots are almost in desired values. They are below 30  $\mu$ m pixel pitch. Dome material should be sapphire because of the aerodynamic effects that acts on dome such as thermal, acceleration. The dome must be durable to these effects. As a result dome material was chosen as a sapphire and Hammer optimization was done.

Dimensions of dome must be compatible with missile diameter. The diameter of missile was assumed as 140 mm before. So that first surface radius of the dome must be 70 mm and according to chosen thick second surface radius must be first surface radius minus thickness. Results are shown in Fig. 4.13 and Table 4.9.

Table 4.9 Lens parameters for case 7

	Material	CT (mm)	R1 (mm)	R2 (mm)	Conic Constant
Dome	Sapphire	2	70	68	0
Air	-	2	-	-	-
Lens1	GE_OLD	2.956	38.254	31.104	0
Air	-	2	-	-	-
Lens2	SILICON	3.922	33.253	51.532	0.088 Second Surface
Air	-	33.72	-	-	-
Lens3	CDSE	2.001	61.932	69.817	-15.917 First Surface
BFL	-	21.4	-	-	-

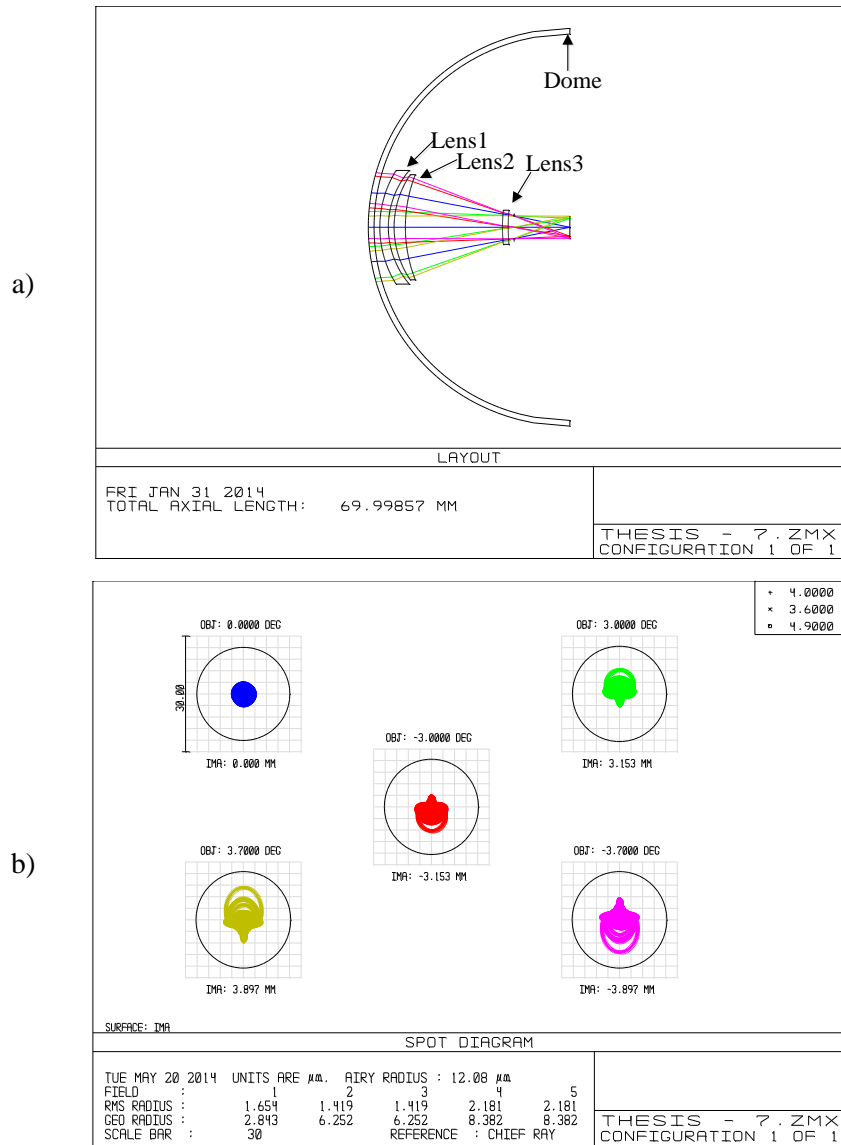


Figure 4.13 Zemax simulations for case 7; a) optical system, b) spot sizes for different fields.

As in Fig. 4.13 and Table 4.9 dome does not have significant effect on optical system. Optical system has reached desired values with dome.

### 4.3 Optical System Performance Parameters

According Rayleigh criteria for aberrations except distortion must below  $0.25\lambda$  for a good imaging system [15]. Parameters are shown in Fig. 4.14. For  $0^\circ$  field,

aberrations are below  $0.1 \lambda$ , for  $3^\circ$  field aberrations below  $0.05 \lambda$  and for  $3.7^\circ$  field aberrations are below  $0.1 \lambda$ .

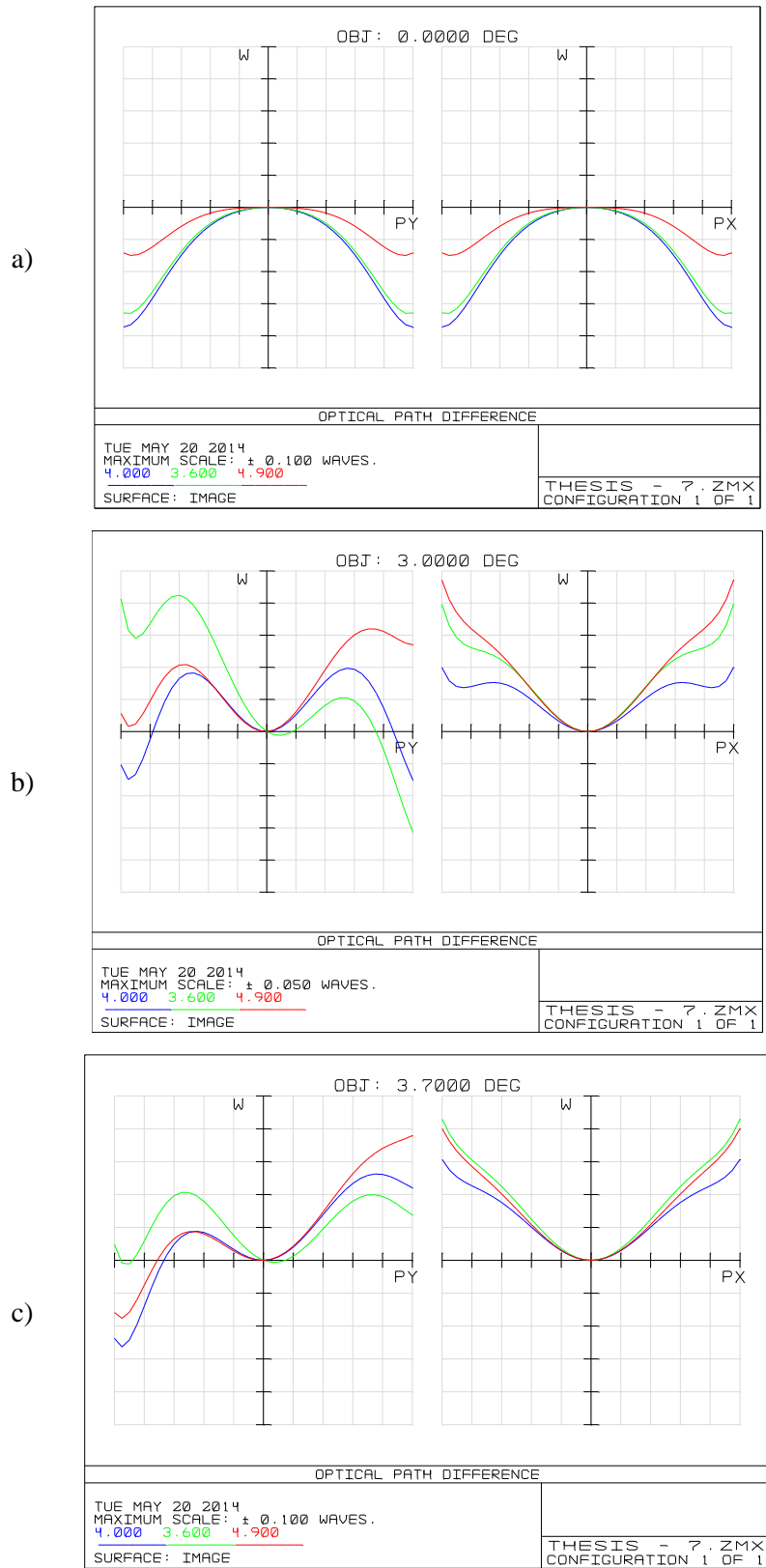
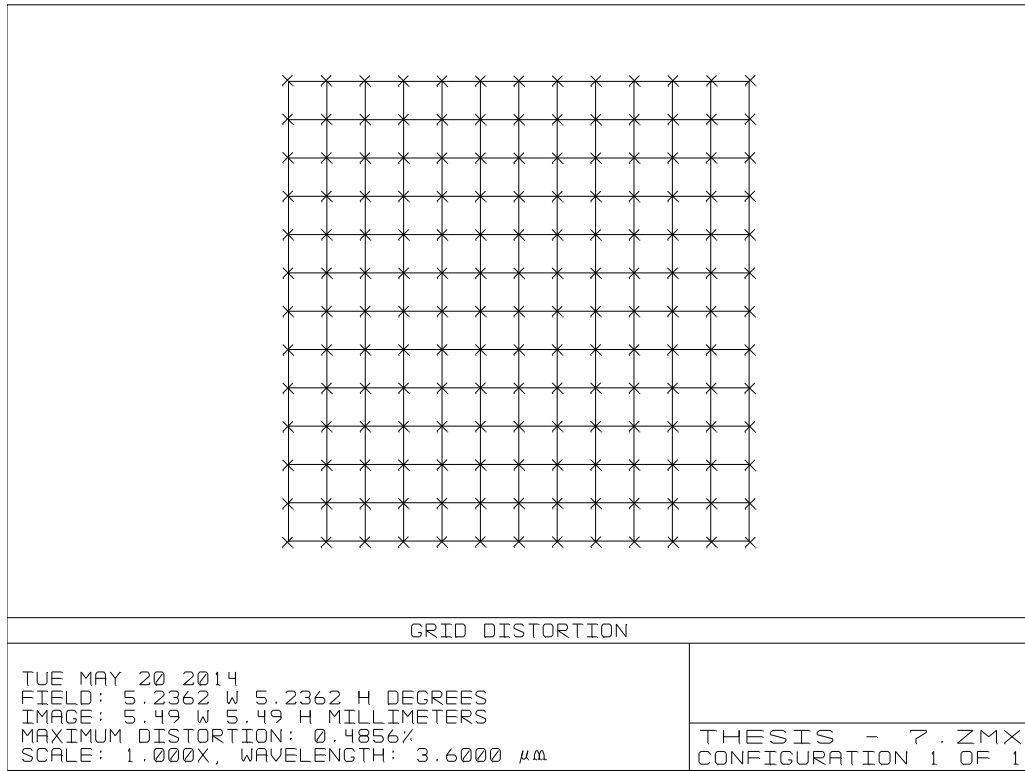


Figure 4.14 OPD of the optical system a)  $0^\circ$  field, b)  $3^\circ$  field and c)  $3.7^\circ$  field

Distortion figures are shown in Fig. 4.15. For 3.6  $\mu\text{m}$  wavelength, distortion is % 0.4856 and for 4.9  $\mu\text{m}$  wavelength distortion is % 0.4841. They are below % 2 distortion criteria and distortion is positive both maximum and minimum wavelengths.

a)



b)

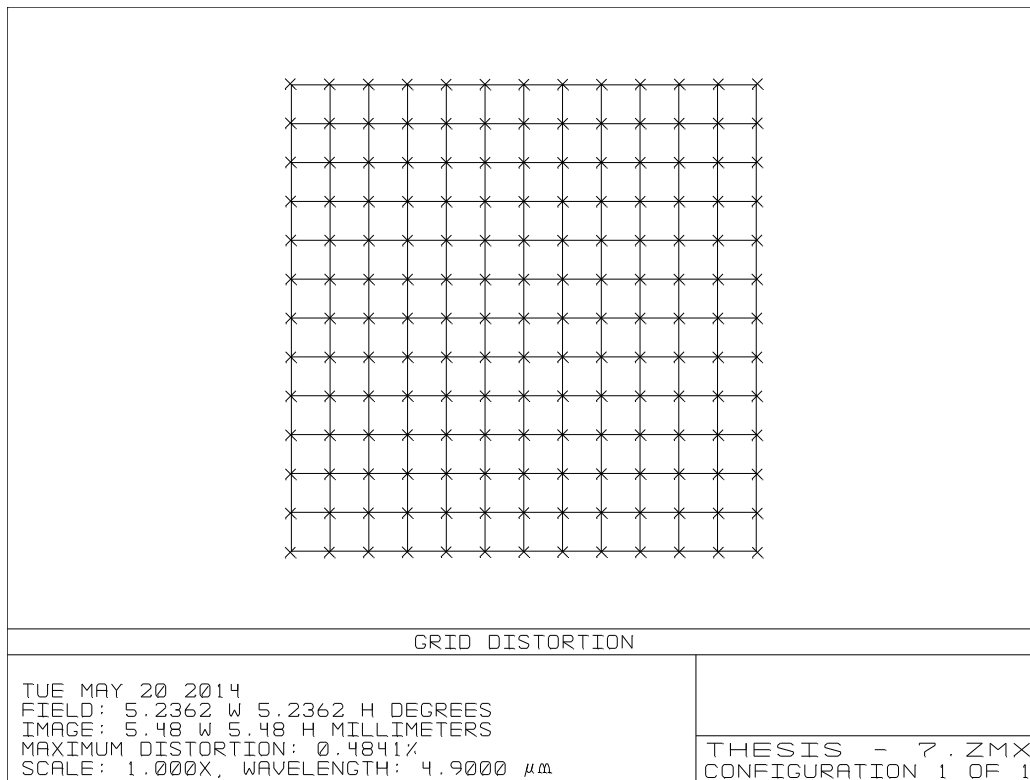


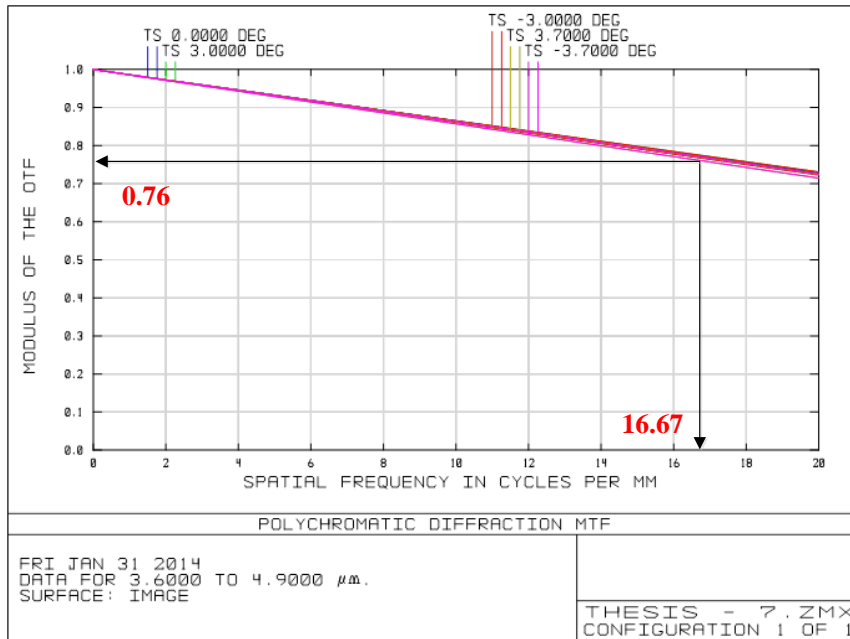
Figure 4.15 Distortion of the optical system

MTF is the most important system performance criteria for an optical system. It shows how the optical system performs between scene and detector.

As shown Fig. 4.16 a) 0.76 portion of target and background signal will be transferred to the detector. If the background radiation is neglected, because  $P_{\text{target}} \gg P_{\text{background}}$  0.76 portion of target signal will pass. MTF was calculated for one black line, means minimum intensity and for one white line, means maximum intensity. Calculation is  $\frac{1}{2} * 0.030\text{mm} = 16.67\text{line/mm}$ .

MTF value below 0.1, optical system does not give an image of scene. This critical value was found from the graph as shown in Fig. 4.16.

a)



b)

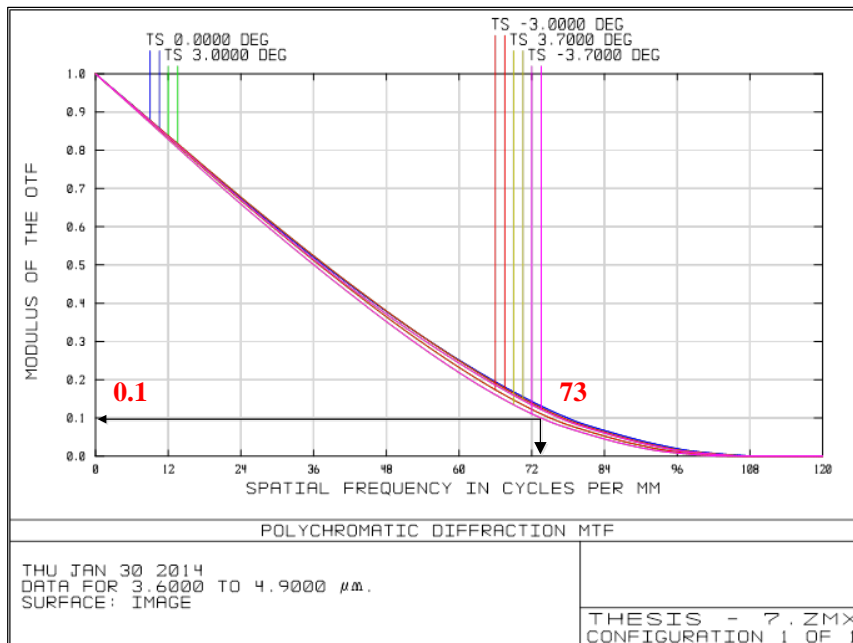


Figure 4.16 MTF of the optical system

## CHAPTER 5

### DISCUSSION AND CONCLUSION

In this study, imaging infrared seeker was designed. Firstly, spectral band of the system was analyzed. Since target was chosen as an aircraft and target temperature was 750 K, the spectral band of the system was taken as MWIR. Atmospheric effects are found from literature because there was no chance to make modeling with MODTRAN software. Therefore, MWIR detector parameters were provided from off-the-shelf products. Then, detection range equations for 5000 m distance were determined considering 750 K target radiation and 283 K background radiation and these equations were programmed with C# programming language.

After detection range calculations, optical system parameters and performance criterions were defined. Focal length of the system was calculated as 60 mm and  $F_{\#}$  is below 3. Resolution criterion in focal plane is detector pixel size.

While doing this optical design Zemax software was used. Merit function editor was used to restrict the optical system such as 60 mm focal plane, 70 mm total length, etc, while doing optimization and Hammer optimization. Simulations of optical system were done for different fields.

To obtain near diffraction limited system, 4 different types of glass were used. Sapphire is dome material and it was not optimized. For Lens1, Ge\_Old lens was used. For Lens2, Silicon lens was used and for Lens3, CdSe lens material was used. These material types were determined while Hammer optimization. Before

optimization, usable infrared materials must be determined because some lens materials cause problems. For example NaCl glass melts under moist conditions.

OPD plots were drawn for different fields and for different wavelength. The optical system satisfies the Rayleigh resolution criterion and distortion is below %2 for maximum and minimum wavelength.

To manufacture of this optics test plate fitting must be done to be manufactured company. “Edmund Optics Inc.” is chosen to test the manufacturability. Test plate fitted parameters are shown in Table 5.1.

Table 5.1 Lens parameters after test plate fitting

	Material	CT (mm)	R1 (mm)	R2 (mm)	Conic Constant
Dome	Sapphire	2	70	68	0
Air	-	2	-	-	-
Lens1	GE_OLD	2.956	38.354	31.318	0
Air	-	2	-	-	-
Lens2	SILICON	3.922	33.350	51.460	0.088 Second Surface
Air	-	33.72	-	-	-
Lens3	CDSE	2.001	61.849	69.790	-15.917 First Surface
BFL	-	21.4	-	-	-

OPD for 0° field, aberrations are below 0.1 λ, for 3° field aberrations below 0.1 λ and for 3.7° field, aberrations are below 0.1 λ. Only difference comes from 3° field. But it is again below the Rayleigh criteria.

Distortion is %0.4722 for 3.6 μm and %0.4705 for 4.9 μm.

MTF is 0.76. It is same before test plate fitting.

Space is limited with the missile diameter. Seeker's optics must be settled in this geometry. As a result, total length of the seeker's optics must not exceed 70 mm for 140 mm diameter missile.

To sum up, imaging infrared seeker analysis was done for aerial targets at 5000 m distance. Test plate fitted configuration is convenient to manufacture because system performance does not degrade significantly. It satisfies system requirements after all.

Although the results presented here is effective, for more cost effective solution of the seeker optics, optimization processes can be repeated. Manufacturing coast can be reduced because the seeker is one of the high-priced parts of a missile.



## REFERENCES

1. Bruce H. Walker, *Optical Engineering Fundamentals*, SPIE Press, 2008, pp 112-113.
2. Canada Research Chair  
<http://mivim.gel.ulaval.ca/dynamique/index.php?idD=58&Lang=1>  
Retrieved on 13 October 2013
3. Arnold Daniels, *Field Guide to Infrared Systems*, SPIE Press, 2007, pp 1-50
4. Aerospaceweb.org  
<http://www.aerospaceweb.org/question/electronics/q0191.shtml>  
Retrieved on 16 January 2014
5. Helmut Budzier and Gerald Gerlach, *Thermal Infrared Sensors Theory Optimisation and Practice*, WILEY, Germany, 2011, pp 117-121
6. A. Rogalski and K. Chrzanowski, “*Infrared Devices and Techniques*”, *Opto-Electronics Review*, 2002, Vol. 10, pp 111-136
7. Bakshi, U. A. and Godse, A. P. *Basic Electronics Engineering*, 2009, Technical Publications. pp. 8–10.
8. Song, T.L, “*Target Adaptive Guidance for Passive Homing Missiles*”, 1997, *IEEE*, Vol. 33, Issue 1, pp 312-316.
9. David H. Pollock, *The Infrared & Electro-Optical Systems Handbook, Countermeasure Systems*, Vol. 7, 1999.
10. Shripad P. Mahulikar, Hemant R. Sonawane, G. Arvind Rao “*Infrared Signature Studies of Aerospace Vehicles*”, 2007, *Science Direct*, Vol. 43, Issue 7-8, pp 218-245.

11. Sang-Ho Ahn, Young-Choon Kim, Tae-Wuk Bae, Byoung-Ik Kim, Ki-Hong Kim, “*DIRCM Jamming Effect Analysis of Spin-Scan Reticle Seeker*”, Communications (MICC), 2009 IEEE 9th Malaysia International Conference on, pp 183-186.
  
12. Tae-Wuk Bae, Byoung-Ik Kim, Young-Choon Kim, Sang-Ho Ahn, “*Jamming effect analysis of infrared reticle seeker for directed infrared countermeasures*”, 2012, Infrared Physics & Technology, Vol. 55, Issue 5, pp 431–441.
  
13. Surng-Gabb Jahng, Hyun-Ki Hong, Sung-Hyun Han, Jong-Soo Choi, “*Dynamic simulation of the rosette scanning infrared seeker and an infrared counter countermeasure using the moment technique*”, 1998, SPIE Optical Engineering, Vol. 38, Issue 5, pp 921-928.
  
14. Ehsan Rahimi, Shahriar B. Shokouhi, “*A Parallelized and Pipelined Datapath to Implement ISODATA Algorithm for Rosette Scan Images on a Reconfigurable Hardware*”, 2007, IEEE, p 433.
  
15. Robert E. Fischer, Biljana Tadic-Galeb, Paul R. Yoder, *Optical System Design*, Second Edition, pp 29-90
  
16. O. Neshor, S. Elkind, G. Francis, M. Kenan, “*SCD Solutions for Missile Warning Systems*”, 2006, SPIE, Vol. 6206
  
17. Ajay Kumar and S.S. Negi “*Design and Development of High Performance 3<sup>rd</sup> Generation Hand Held Thermal Camera*”, 2004, SPIE, Vol. 5563
  
18. Peter Y. Yu and Manuel Cardona, *Fundamentals of Semiconductors Physics and Materials Properties*, Springer Press, 2010. p. 310.
  
19. Standart Test Method for Noise Equivalent Temperature Difference of Thermal Imaging Systems, ASTM International, Designation E1543-00.

20. Ab-Rahman and Mazen R. Hassan, Mohammed Syuhaimi, “*Lock-on Range of Infrared Heat Seeker Missile*”, 2009, Electrical Engineering and Informatics, 2009, International Conference on, Vol. 02, pp 472 – 477.
21. Donald E. McCharty “The Reflection and Transmission of Infrared Materials: I, Spectra from 2 50 Microns”, Applied Optics, Vol. 2, Issue 6, pp 591-595.
22. Max J. Riedl, *Optical Design Applying the Fundamentals*, SPIE, 2009.
23. Robert E. Fischer, R. Barry Johnson, Warren J. Smith “*Scalable MWIR and LWIR optical system designs employing a large spherical primary mirror and small refractive aberration correctors*” 2001, SPIE, Vol. 4441.



## APPENDIX A

### SOFTWARE CODES OF “INFRARED RANGE AND NETD CALCULATOR”

“*Infrared Range and NETD Calculator*” software programming (C#) codes;

```
using System;
using System.Collections.Generic;
using System.ComponentModel;
using System.Data;
using System.Drawing;
using System.Linq;
using System.Text;
using System.Windows.Forms;

namespace NETD
{
    public partial class Form1 : Form
    {
        double NETD;
        double lambda2;
        double lambda1;
        double Toptics;
        double PixelPitch;
        double FNumber;
        double EmissivityBack;
        double Tbackground;
        double NEP;
        double CalculationSensitivity;
        double DetectorAbsorbtion;

        // constants;

        double h;
        double k;
        double c;

        // Detection Range

        double DetectionRange;
        double ExtinctionCoefficient;
        double TargetArea;
        double BackgroundArea;
        double TargetTemperature;
        double TargetEmissivity;
    }
}
```

```

double BackTemperature;
double BackEmissivity
double Focallength;
double AtmosphericTrans;
double ClearAperture;
double PowOnDetTarget;
double PowOnDetBack;

public Form1()
{
    InitializeComponent();
    h = 6.62606957 * Math.Pow(10, -34); // J.s
    c = 3 * Math.Pow(10, 8); // m/s
    k = 1.3806488 * Math.Pow(10, -23); // J/K
}

private void button1_Click(object sender, EventArgs e)
{
    NETD = double.Parse(textBox1.Text) * Math.Pow(10, -3);
    lambda2 = double.Parse(textBox3.Text) * Math.Pow(10, -6);
    lambda1 = double.Parse(textBox4.Text) * Math.Pow(10, -6);
    Tbackground = double.Parse(textBox5.Text) ;
    Toptics = double.Parse(textBox6.Text);
    PixelPitch = double.Parse(textBox7.Text) * Math.Pow(10, -6);
    FNumber = double.Parse(textBox8.Text);
    EmissivityBack = double.Parse(textBox9.Text);
    CalculationSensitivity = double.Parse(textBox10.Text);
    DetectorAbsorbtion = double.Parse(textBox11.Text);
    NEP = NETD * DerivativeExitanceCalculator(Tbackground, lambda2,
lambda1, EmissivityBack, CalculationSensitivity, DetectorAbsorbtion) *
Math.Pow(PixelPitch, 2) * Toptics / (4 * Math.Pow(FNumber, 2) + 1);
    textBox2.Text = NEP.ToString();
}

public double DerivativeExitanceCalculator(double Temperature, double
Lambda2, double Lambda1, double emissivity, double Sensitivity, double
Absorbtion)
{
    double h = 6.62606957 * Math.Pow(10, -34); // J.s
    double c = 3 * Math.Pow(10, 8); // m/s
    double k = 1.3806488 * Math.Pow(10, -23); // J/K
    double[] Lambda;
    double[] sabit;
    double[] fonk;
    double integral = 0;
    int ArrayLength = Convert.ToInt32((lambda2 - lambda1) *
Math.Pow(10, 6) * Sensitivity) + 1;
    Lambda = new double[ArrayLength];
    sabit = new double[ArrayLength];
    fonk = new double[ArrayLength];
    Lambda[0] = lambda1;
    for (int i = 1; i < Lambda.Length ; i++)
    {
        Lambda[i] = Lambda[0] + (double)i * (lambda2 - lambda1) /
Lambda.Length;
    }
}

```

```

        for (int i = 0; i < Lambda.Length ; i++)
        {
            sabit[i] = h * c / (Lambda[i] * k * Temperature);
        }
        for (int i = 0; i < Lambda.Length ; i++)
        {
            fonk[i] = emissivity * Absorbtion * (2 * Math.PI * Math.Pow(h,
2) * Math.Pow(c, 3) / (Math.Pow(Lambda[i], 6) * k * Math.Pow(Temperature, 2))
* Math.Exp(sabit[i]) / (Math.Pow((Math.Exp(sabit[i]) - 1), 2)));
        }
        for (int i = 0; i < Lambda.Length-1; i++)
        {
            integral = integral + (Lambda[i + 1] - Lambda[i]) * (fonk[i +
1] + fonk[i]) / 2;
        }
        return integral;
    }

    public double SpectralRadianceExitance(double lambda2, double lambda1,
double Temperature, double emissivity, double Sensitivity)
    {
        /// (W/m2-µm)
        double h = 6.62606957 * Math.Pow(10, -34); // J.s
        double c = 3 * Math.Pow(10, 8); // m/s
        double k = 1.3806488 * Math.Pow(10, -23); // J/
        double[] Lambda;
        double[] sabit;
        double[] fonk;
        double integral = 0;
        int ArrayLength = Convert.ToInt32((lambda2 - lambda1) *
Math.Pow(10, 6) * Sensitivity) + 1;
        Lambda = new double[ArrayLength];
        sabit = new double[ArrayLength];
        fonk = new double[ArrayLength];
        Lambda[0] = lambda1;
        for (int i = 1; i < Lambda.Length; i++)
        {
            Lambda[i] = Lambda[0] + (double)i * (lambda2 - lambda1) /
Lambda.Length;
        }
        for (int i = 0; i < Lambda.Length; i++)
        {
            sabit[i]= h * c / (Lambda[i] * k * Temperature);
        }
        for (int i = 0; i < Lambda.Length; i++)
        {
            fonk[i] = emissivity * 2 * Math.PI * h * Math.Pow(c, 2) /
(Math.Pow(Lambda[i], 5) * (Math.Exp(sabit[i])-1));
        }
        for (int i = 0; i < Lambda.Length - 1; i++)
        {
            integral = integral + (Lambda[i + 1] - Lambda[i]) * (fonk[i +
1] + fonk[i]) / 2;
        }
        return integral;
    }
}

```

```

private void button2_Click(object sender, EventArgs e)
{
    CalculationSensitivity = double.Parse(textBox20.Text);
    DetectionRange = double.Parse(textBox23.Text);
    ExtinctionCoefficient = double.Parse(textBox21.Text) * 100 *
Math.Pow(10, -6);
    TargetArea = double.Parse(textBox24.Text);
    BackgroundArea = double.Parse(textBox25.Text);
    TargetTemperature = double.Parse(textBox22.Text);
    TargetEmissivity = double.Parse(textBox12.Text);
    BackTemperature = double.Parse(textBox13.Text);
    BackEmissivity = double.Parse(textBox14.Text);
    FocalLength = double.Parse(textBox15.Text)/1000;
    lambda2 = double.Parse(textBox27.Text) * Math.Pow(10, -6);
    lambda1 = double.Parse(textBox26.Text) * Math.Pow(10, -6);
    FNumber = double.Parse(textBox17.Text);
    DetectorAbsorbtion=double.Parse(textBox29.Text);
    AtmosphericTrans = Math.Exp(-ExtinctionCoefficient *
DetectionRange);
    ClearAperture = FocalLength / FNumber;
    PowOnDetTarget = DetectorAbsorbtion *
SpectralRadianceExitance(lambda2, lambda1, TargetTemperature,
TargetEmissivity, CalculationSensitivity) * TargetArea *
    Math.Pow(ClearAperture / 2, 2) * Toptics * AtmosphericTrans /
Math.Pow(DetectionRange, 2);
    PowOnDetBack =DetectorAbsorbtion *
SpectralRadianceExitance(lambda2, lambda1, BackTemperature, BackEmissivity,
CalculationSensitivity) *
    BackgroundArea * Math.Pow(ClearAperture / 2, 2) * Toptics *
AtmosphericTrans / Math.Pow(DetectionRange, 2);
    textBox18.Text = PowOnDetTarget.ToString();
    textBox19.Text = PowOnDetBack.ToString();
    textBox28.Text = NEP.ToString();
    textBox30.Text = Math.Round((PowOnDetTarget / NEP),3).ToString();
    textBox16.Text = Math.Round((PowOnDetBack / NEP),3).ToString();
    textBox31.Text = (SpectralRadianceExitance(lambda2, lambda1,
TargetTemperature, TargetEmissivity, CalculationSensitivity) /
SpectralRadianceExitance(lambda2, lambda1, BackTemperature, BackEmissivity,
CalculationSensitivity)) .ToString();
    led1.Value = true;
}
}
}

```